Remote Sensing Solutions, Inc.

PROJECT: Operational SFMR-NAWIPS Airborne Processing and Data Distribution Products

NOAA Award No.: NA05OAR4171101

Annual Report: Year 1

Prepared By: Dr. James Carswell

Date: 07/10/2006

TABLE OF CONTENTS

1 INTRODUCTION

1.1 SCOPE

This document reports on the first year activities of the Joint Hurricane Testbed (JHT) project entitled, "Operational SFMR-NAWIPS Airborne Processing and Data Distribution Products," and recommends the activities that should occur during the second year.

1.2 GOAL

To provide the reader with background information on the proposed effort, describe the accomplishments of the work performed and present the recommendations for the second year activities, which will build off those in the first year.

1.3 DOCUMENT BREAKDOWN

This document contains four sections. Section 1 contains the introduction. Section 2 reviews the objectives of the first year efforts. Section 3 presents the results obtained and the tools developed in the first year. Section 4 discusses the work that should be performed during the second year to fully transition the project to operations.

2 FIRST YEAR OBJECTIVES

In accordance with the proposal and approved schedule for this JHT project, the first year effort was to: 1) develop and document an operational calibration and tuning process for the AOC SFMR instruments, 2) evaluate and develop processes to ensure sea surface temperature (SST) is properly handled in the operational retrieval process, 3) evaluate the SFMR GMF and quality of the retrievals, 4) evaluate bathometry effects with the limited 2005 data set and recommend next steps, 5) evaluate and implement initial processes for identifying and flagging land and RFI contamination and 6) evaluate second year objectives and work plan based on the first year results. Since the land flagging routine had already been implemented within the ProSensing processor, it was not investigated. NOAA HRD, through supplemental funding, performed an in depth validation effort comparing the AOC SFMR wind retrievals to GPS dropsonde measurements. Therefore this effort did not duplicate this comparison.

3 FIRST YEAR ACTIVITIES / RESULTS

Below the activities and results of the first year effort are presented.

3.1 AOC SFMR Calibration / Tuning

The AOC SFMR instrument, designed and fabricated by ProSensing, Inc., is to provide accurate, real-time near ocean surface wind speed and rain rate

estimates of tropical storms and cyclones from the NOAA WP-3D aircraft, and in the future, from the 53rd Air Force Reserve WC-130 aircraft. This instrument does not directly measure these parameters, but rather measures the emission of the ocean surface and precipitation within its field of view. The near ocean surface wind speed and the column averaged rain rate are inferred from these measurements. To estimate the wind speed and rain rate, a geophysical model function (GMF) is used. The GMF predicts the dependence of C-band brightness temperature measurements to the 10-m ocean surface wind speed and to the column averaged rain rate. Using this GMF, a retrieval process determines the ocean surface wind speed and rain rate combination that best describes the brightness temperature measurements. Figure 1 and Figure 2 plot the brightness temperature dependence on the 10-m ocean surface wind speed and column averaged rain rate as predicted by the GMF. This figure shows:

- The predicted brightness temperature measurements increase with ocean surface wind speed, and this relationship is weakly dependent on frequency.

- The predicted brightness temperature measurements increase with rain rate, and this dependence is strongly dependent on frequency.

Using these relationships, the retrieval process detects the presence of rain by evaluating the difference in the brightness temperature measurements as a function of frequency and estimates the ocean surface wind speed from the mean brightness temperature response. Of course, this description is an over simplification of the process, since both wind and rain will cause the mean brightness temperature to increase. However, it is the difference in the frequency dependence that allows the retrieval process to estimate both the wind speed and rain rate. Additionally this will cause the wind and rain retrievals to be sensitive to different types of errors as will be shown later in this section.

Besides being required to separate the wind signature from the rain signature, the retrieval process is also challenged by the accuracy of the measurements and the GMF. That is, the AOC SFMR does not report the true brightness temperature, but rather outputs voltages. An empirically derived calibration transfer function is used to map these voltages to brightness temperature measurements. Errors in this transfer function will result in retrieval errors. Likewise, the GMF used by the retrieval process was also derived empirically, and thus contains errors / offsets.

To overcome these shortcomings, the AOC SFMR must be calibrated or "tuned" to the GMF. This is a common practice in satellite remote sensing applications to eliminate potential biases between the GMF and the measurements. This calibration / tuning process will be discussed later. First, the sensitivity of the retrieval process to errors in the calibration, tuning and/or GMF is presented in order to better understand the requirements on this tuning process.
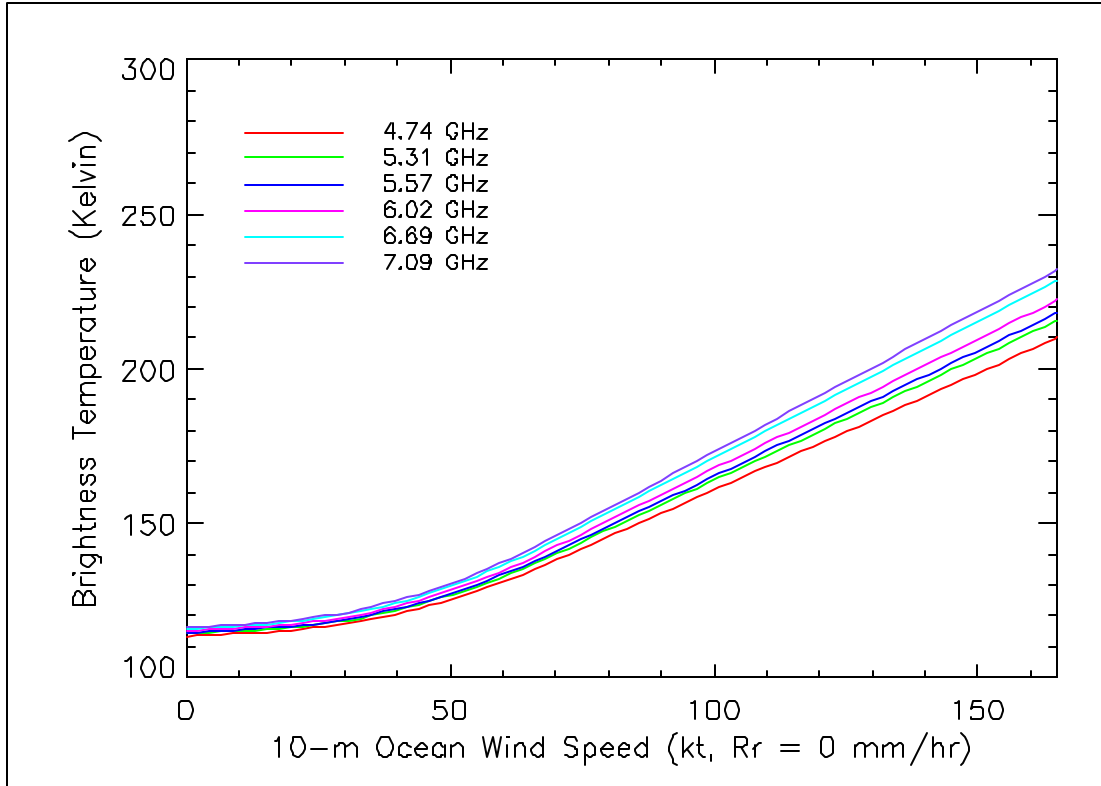
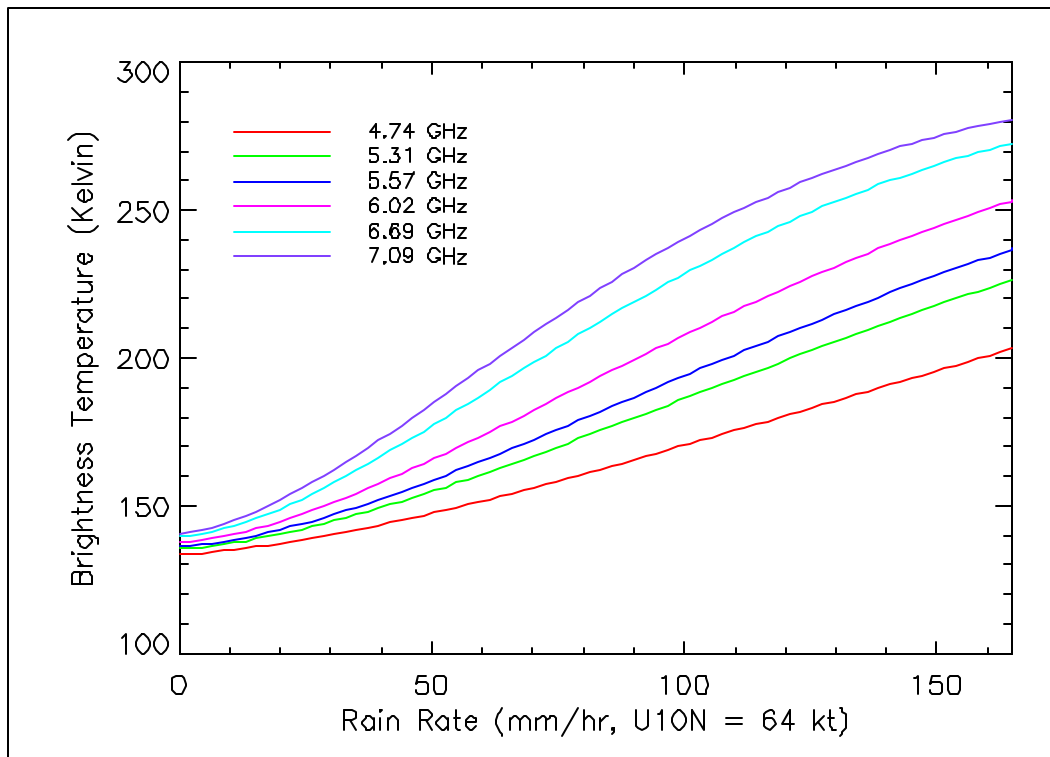**Figure 1: Brightness temperature versus wind speed.**

Figure 2: Brightness temperature versus rain rate.

3.1.1 Sensitivity of the SFMR Retrieval Process on Calibration

To determine the sensitivity of the SFMR retrieval process to the accuracy of the SFMR calibration or tuning, the JHT SFMR team built a software simulator that models the full SFMR measurement and retrieval process and allows the sensitivity of this process to various parameters to be studied. Figure 3 presents a high level diagram of the simulator. It consists of three primary engines. The first generates brightness temperature estimates using the SFMR GMF. Information about the platform and environment (including wind speed and rain rate) can be inputted into the GMF. The various parameters governing the rain and ocean surface emissivity and absorption can also be controlled / modified in order to study the sensitivity of the retrieval process to the GMF itself. The second engine models the instrument (measurement precision and sampling) and errors in the calibration / tuning process and generates a specified number of realizations (i.e. Monte-Carlo simulation). The third engine implements the retrieval process which uses the SFMR GMF. Both the retrieval code and the GMF were verified line by line with the real-time retrieval code used by AOC and the post processing retrieval code used by HRD to ensure there were no differences. The GMF in the retrieval code is also the same GMF that is used in the first engine but its parameters are fixed to those values used by the AOC real-time processor.

For a typical simulation run, five hundred to one thousand independent realizations are produced at seven different wind speeds (33, 50, 64, 83, 96, 114,135 and 165 knots) and six different rain rates (0, 5, 10, 20, 30 and 40 mm/hr). Note that the highest rain rate is only 40 mm/hr. Higher rain rates were not used because previous comparisons between the SFMR rain rate estimates and those derived with the Imaging Wind and Rain Airborne Profile have shown the SFMR to underestimate the rain rate by almost a factor of two. That is, 40 mm/hr is really 80 mm/hr using the current SFMR GMF. From these independent realizations, the mean and standard deviation of the retrieval products are calculated at each wind speed and rain rate (48 different combinations of wind speed and rain rate). Properties of the distribution and the distribution of the retrievals are also calculated. Through this approach, the sensitivity of the SFMR retrieval process to an individual parameter and to errors in this parameter can be studied over wind, rain and measurement space.

Before using the simulator to determine the effects of calibration errors (herein referred to as tuning errors) on the retrieval process, the performance of the simulator was verified over the expected range of wind speeds (0 to 165 knots) and rain rates (0 to 40 mm/hr) to ensure that the estimates derived had a zero mean bias and standard deviations of the retrievals were consistent with the modeled measurement noise (i.e. ΔT).
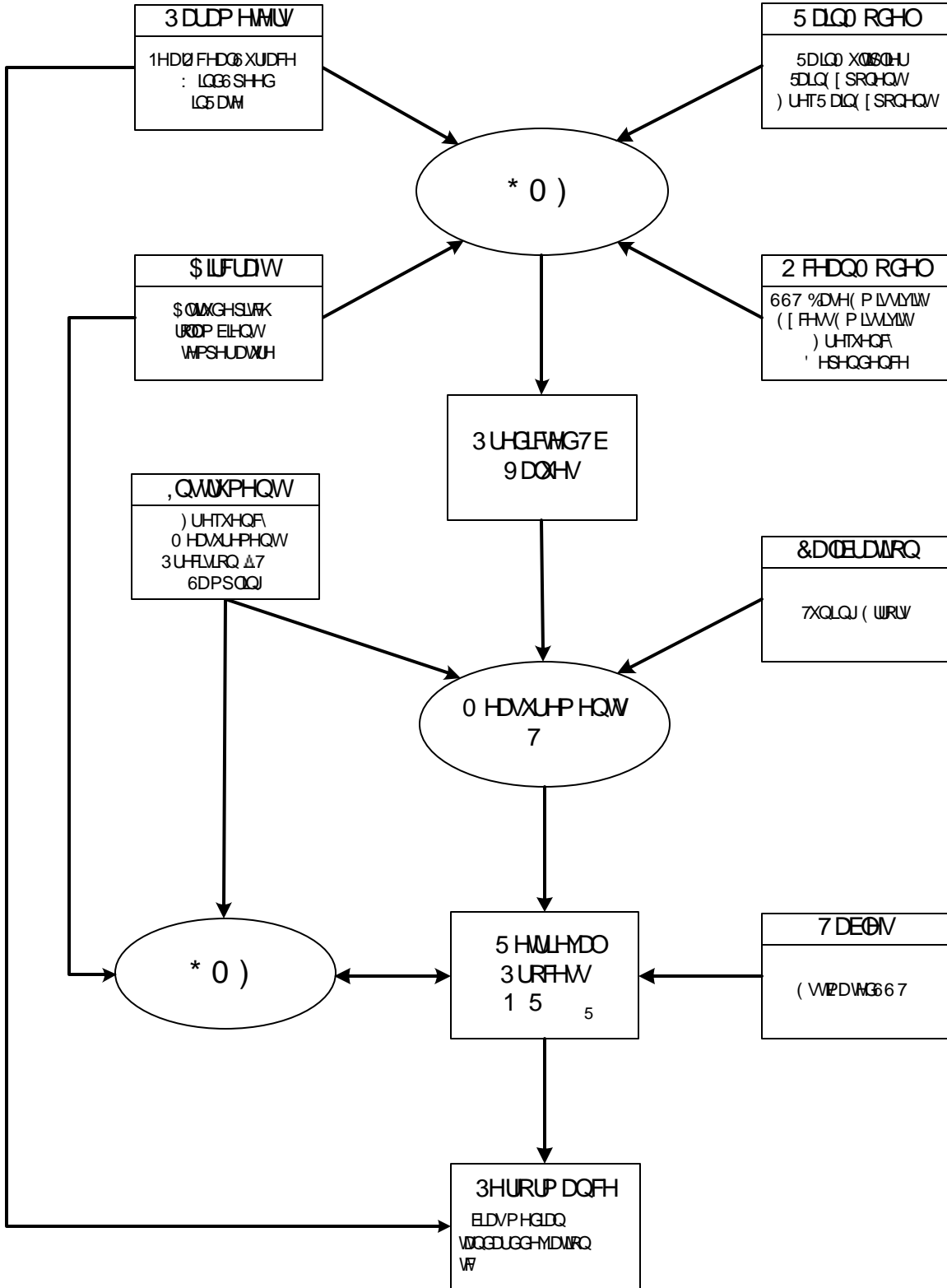
Figure 3: Full SFMR Retrieval Simulator

3.1.1.1   Calibration / Tuning Errors

Working with AOC and ProSensing, the JHT team held several meetings on the calibration procedure and validation. The maximum possible uncertainty in the calibration / tuning (i.e. maximum possible mean difference between the measured brightness temperature and predicted value by the GMF) was estimated by this group to be +/- 1 Kelvin for each frequency channel. Using the simulator, the JHT team evaluated the effect that tuning errors have on the retrieval process. For each iteration of the simulation, different combinations of calibration / tuning errors were introduced while all other parameters were held constant. This evaluation was performed for all wind speed and rain rate combinations. Each channel was allowed to have a tuning error of -1.0, -0.5, 0.0, 0.5 or 1.0 K which resulted in 15,625 different possible combinations of calibration errors, each evaluated for 48 different wind and rain combinations (total of 750,000 cases with each case containing 500 realizations). The step size of 0.5 K was chosen for practical reasons (number of possible combinations equal number of steps raised to the 6th power). In the end, this proved to be more than adequate for determining the acceptable calibration/tuning error. Another interesting result shown by this table is that the mean error in the near ocean surface wind speeds are highly correlated to the mean error in the rain rate estimates (standard deviations are also correlated). In fact for almost all cases, the correlation is around -95 percent, with the exception of 0 mm/hr cases, where the correlation is approximately -88 percent.

To illustrate this relationship, Figure 4 plots the mean error in the near ocean surface wind speed retrieval versus the mean error in the rain rate retrieval for each warning wind speed, 10 mm/hr rain rate and for all possible calibration / tuning errors. The same behavior is seen at all other rain rates as well (for detail plots of all cases, contact carswell@rmss.us). Clearly, when a mean error is present in the wind speed estimate caused by a calibration / tuning error, there is also a corresponding error in the rain rate retrieval and visa versa. This has two important implications:

- The GMF must accurately describe both the wind speed and rain rate dependence. A 1 K error can cause wind speed errors in excess of 10 kts at gale force winds and 6 kts at hurricane force winds.

- The calibration – validation process must verify both the wind and the rain retrievals, whereas past procedures only verified the ocean surface wind retrievals.

Table 1 presents the maximum mean errors (i.e. biases not standard deviations) in the retrievals for the different combinations of wind speed and rain rate. As this table shows, significant errors in the wind speed estimates, even at hurricane force winds, can result even when the calibration tuning error is confined to a 1 K. Of course, one must also remember that this is the maximum possible mean error and not necessarily the true mean error, which will depend on the actual tuning error.

Another interesting result shown by this table is that the mean error in the near ocean surface wind speeds are highly correlated to the mean error in the rain rate estimates (standard deviations are also correlated). In fact for almost all cases, the correlation is around -95 percent, with the exception of 0 mm/hr cases, where the correlation is approximately -88 percent.

To illustrate this relationship, Figure 4 plots the mean error in the near ocean surface wind speed retrieval versus the mean error in the rain rate retrieval for each warning wind speed, 10 mm/hr rain rate and for all possible calibration / tuning errors. The same behavior is seen at all other rain rates as well (for detail plots of all cases, contact carswell@rmss.us). Clearly, when a mean error is present in the wind speed estimate caused by a calibration / tuning error, there is also a corresponding error in the rain rate retrieval and visa versa. This has two important implications:

- The GMF must accurately describe both the wind speed and rain rate dependence. A 1 K error can cause wind speed errors in excess of 10 kts at gale force winds and 6 kts at hurricane force winds.
- The calibration – validation process must verify both the wind and the rain retrievals, whereas past procedures only verified the ocean surface wind retrievals.

Table 1: Maximum retrieval errors caused by 1 K maximum tuning error.

Warning Thresholds	Wind Speed	Rain Rate	Wind Speed Bias		Rain Rate Bias		Correlation
			min	max	min	max	
	knots	mm/hr	knots	knots	mm/hr	mm/hr	%
Tropical Storm Force / Gale	33	0	-12.6	8.9	0.0	4.6	-90.7
	33	5	-11.6	7.8	-3.7	2.4	-93.8
	33	10	-11.3	7.7	-1.9	1.7	-93.7
	33	20	-11.9	7.8	-1.2	1.2	-93.0
	33	30	-13.5	8.3	-1.0	1.1	-92.4
	33	40	-16.0	9.2	-1.1	1.1	-91.8
Storm	50	0	-6.0	5.9	0.0	4.7	-89.3
	50	5	-5.5	5.2	-3.8	2.4	-94.4
	50	10	-5.6	4.9	-2.0	1.8	-94.2
	50	20	-5.8	5.0	-1.2	1.3	-93.4
	50	30	-6.3	5.4	-1.1	1.2	-92.8
	50	40	-7.2	6.0	-1.1	1.2	-92.4
Hurricane Category 1	64	0	-4.3	4.6	0.0	4.9	-89.0
	64	5	-4.0	4.0	-4.3	2.6	-94.5
	64	10	-4.1	3.9	-2.1	1.9	-94.3
	64	20	-4.2	3.9	-1.3	1.4	-93.6
	64	30	-4.6	4.2	-1.2	1.2	-93.0
	64	40	-5.2	4.7	-1.2	1.3	-92.6
Hurricane Category 2	83	0	-3.8	4.4	0.0	5.3	-88.6
	83	5	-3.5	3.9	-4.6	2.9	-94.7
	83	10	-3.5	3.6	-2.4	2.1	-94.6
	83	20	-3.6	3.8	-1.5	1.6	-93.8
	83	30	-4.0	4.2	-1.5	1.5	-97.3
	83	40	-4.5	4.6	-1.4	1.4	-92.9
Hurricane Category 3	96	0	-3.8	4.5	0.0	5.6	-88.6
	96	5	-3.7	4.1	-4.8	3.2	-94.8
	96	10	-3.6	3.8	-2.7	2.3	-94.8
	96	20	-3.7	3.8	-1.8	1.7	-94.0
	96	30	-4.1	4.1	-1.5	1.6	-93.5
	96	40	-4.5	4.6	-1.5	1.6	-93.2
Hurricane Category 4	114	0	-3.9	4.8	0.0	6.2	-88.8
	114	5	-3.7	4.4	-4.9	3.6	-95.1
	114	10	-3.7	3.9	-3.3	2.7	-95.1
	114	20	-3.8	3.8	-2.1	2.0	-94.4
	114	30	-4.1	4.2	-1.8	1.8	-93.9
	114	40	-4.7	4.7	-1.8	1.9	-93.5
Hurricane Category 5	135	0	-4.1	5.0	0.0	7.1	-88.8
	135	5	-3.9	4.7	-4.9	4.4	-95.7
	135	10	-3.9	4.1	-4.3	3.3	-95.5
	135	20	-4.0	4.1	-2.6	2.5	-94.9
	135	30	-4.3	4.4	-2.3	2.2	-94.4
	135	40	-4.5	4.7	-1.8	1.8	-92.9
Maximum Wind	165	0	-4.5	6.2	0.0	9.2	-88.7
	165	5	-4.3	5.8	-4.9	6.2	-95.9
	165	10	-4.3	4.8	-8.1	4.8	-96.2
	165	20	-4.4	4.6	-4.2	3.6	-95.9
	165	30	-4.8	4.9	-3.6	3.3	-95.5
	165	40	-5.5	5.4	-3.5	3.4	-95.3

To better understand the impact of the calibration error, Figure 5 plots the mean bias of the wind speed and rain rate retrievals versus the average calibration error for 114 knots and 10, 20, 30 and 40 mm/hr. Each plot contains the 15,625 different possible combinations of calibration errors. The average calibration error (x-axis) is defined as the average of the calibration errors of each of the channels. In other words, if all channels had a 1 K error, the average calibration area would be 1 K. If the two channels had a -1 K error and four channels had a 1 K error, the average calibration error would be 2/3 K. Note these points should not be thought of as a distribution or scatter. Based on the actual tuning error, only one point would reside in the end. These plots just illustrate the possible errors. For example, the largest positive wind speed error occurs when the upper two frequency channels have a -1 K error and the lower four frequency channels have a +1 K bias. Likewise the most negative wind speed bias comes from just the opposite situation, the upper two frequency channels are biased +1 K high relative to the GMF and the lower four are biased -1 K low from the GMF.

To estimate the maximum tuning error that can be tolerated the wind speed and rain rate estimates are plotted versus the average of the absolute calibration error (average of the absolute value of calibration error in each channel). From this plot, the tuning error must be less than 0.2 K to ensure that the absolute mean error in the wind speed is less than 1 knot. (The results for other rain rates are the same. Contact carswell@rmss.us for detailed plots of all conditions.)
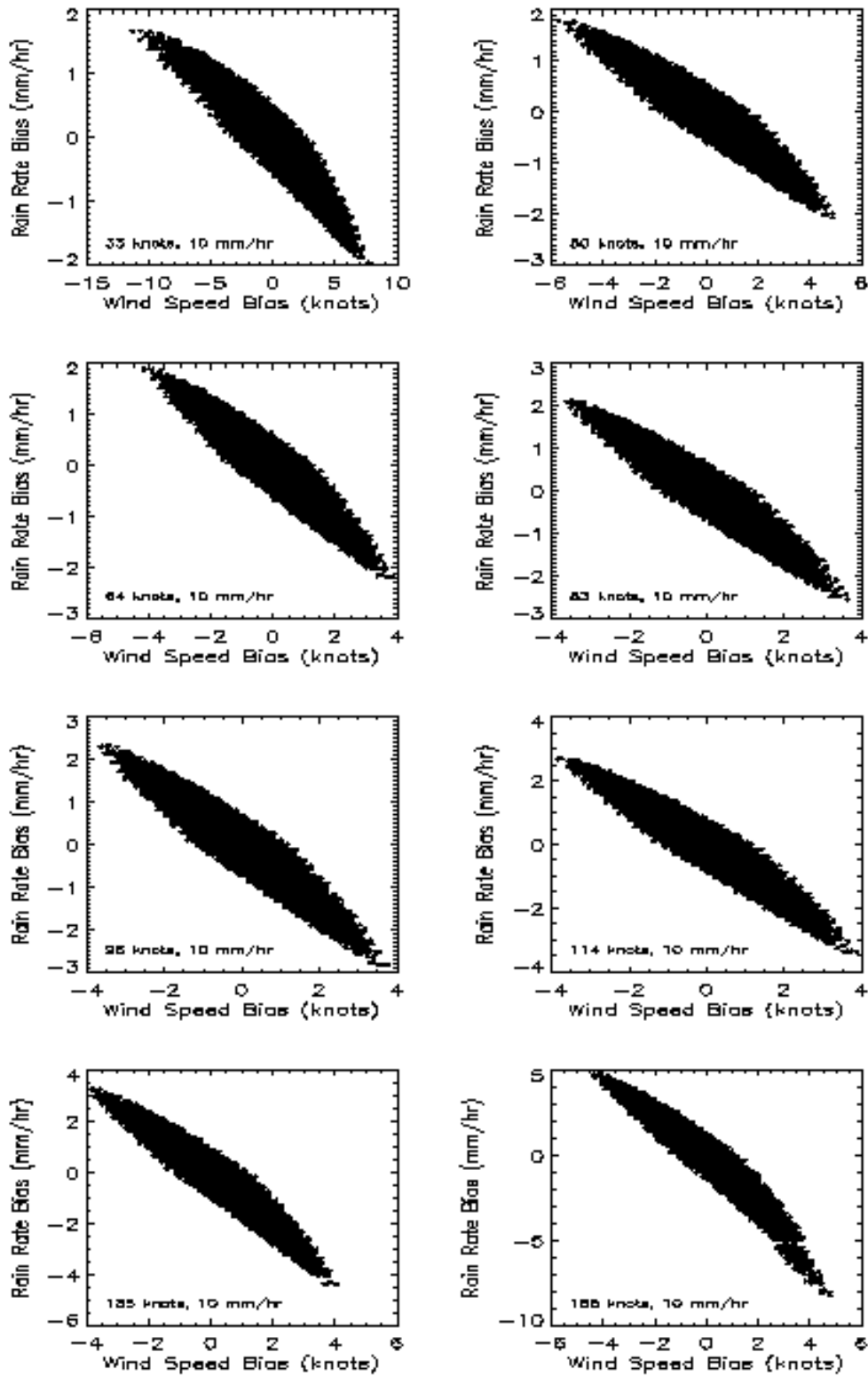
Figure 4: Rain rate retrieval bias plotted versus ocean surface wind retrieval bias (1 K maximum calibration / tuning error).
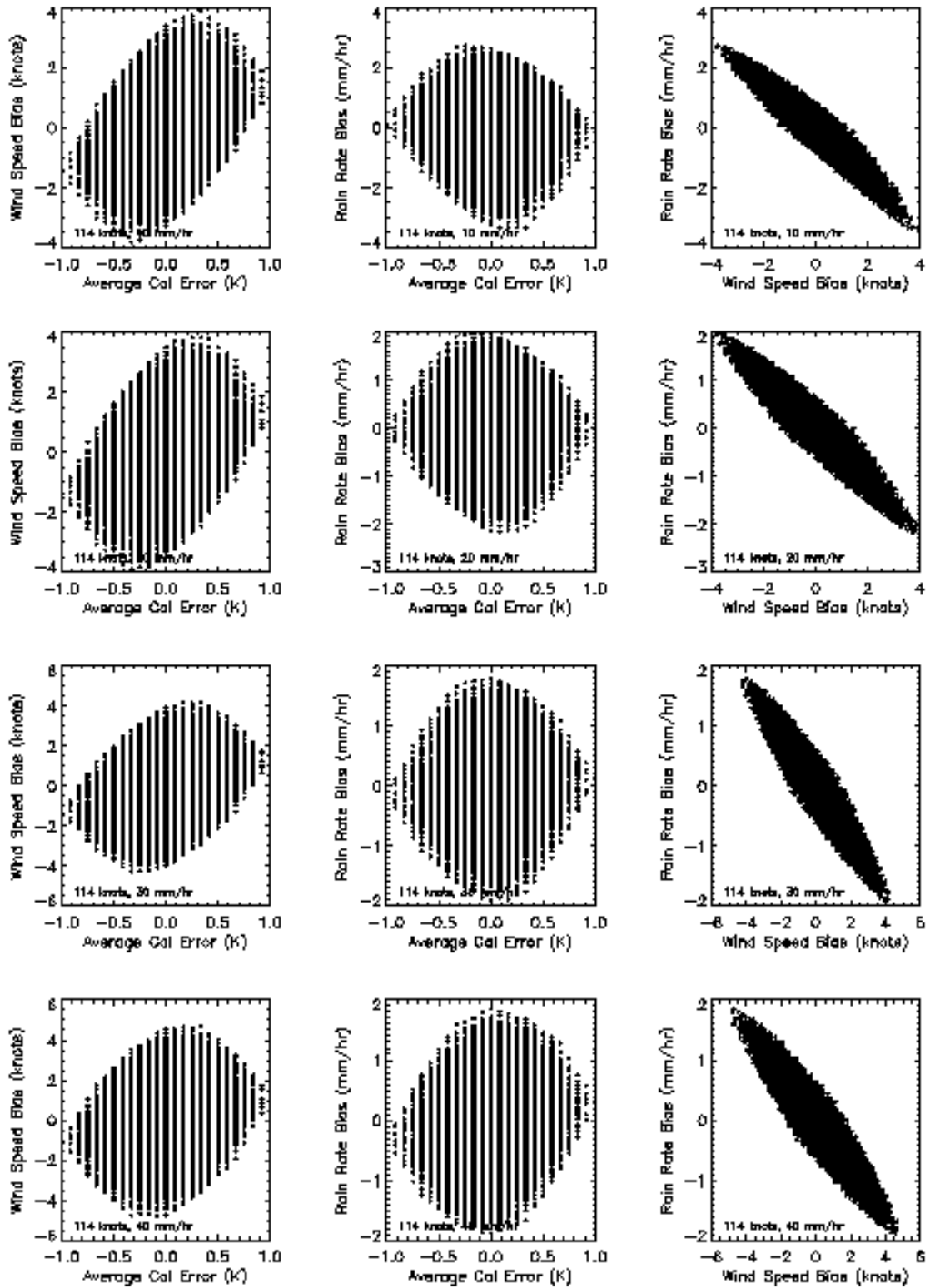
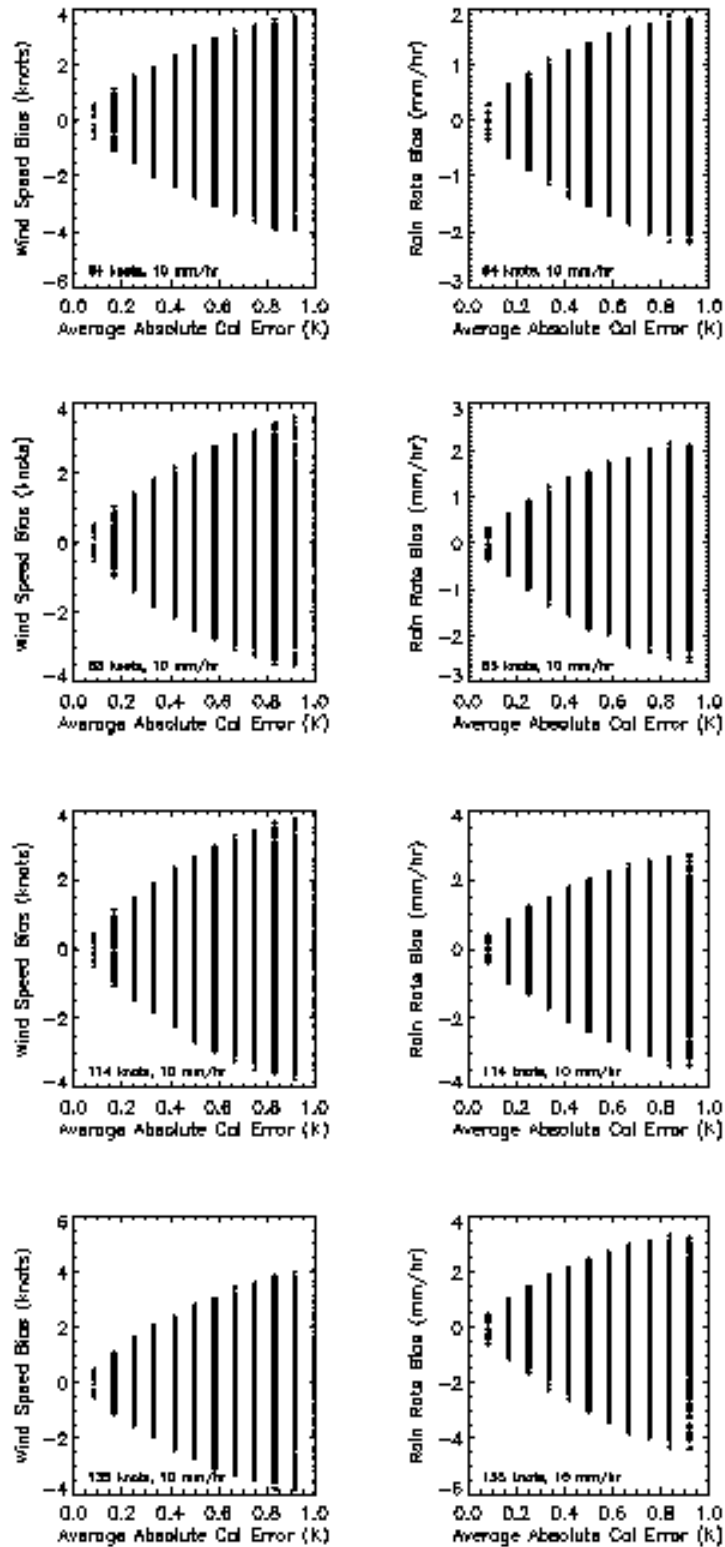**Figure 5: Retrieval errors caused by calibration / tuning errors.**

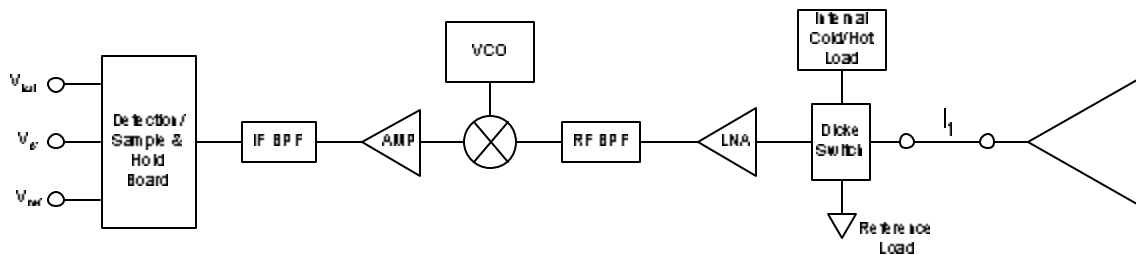**Figure 6: Wind speed and rain retrieval errors versus average calibration error (10 mm/hr).**

3.1.2 Initial Calibration Technique

Tuning the AOC SFMR calibration to within 0.2 K of the GMF (requirement to ensure the absolute mean wind speed error is less than 1 knot) is a difficult task. Because the instrument needs to be calibrated to the GMF, rather than a standard load, the traditional "lab bench" calibration is not appropriate. To overcome this issue, the JHT SFMR team developed an automated calibration technique that would enable the instrument to be automatically calibrated while installed on the aircraft.

Figure 7 presents an over simplified block diagram of the AOC SFMR. Because of the restrictions placed on proprietary information of ProSensing, Inc, a detailed block diagram was unavailable. With these restrictions, the JHT SFMR team could neither obtain nor present such a diagram in this report. Nevertheless, for this discussion the simplified diagram shown below should more than suffice. To understand the automatic calibration "tuning" algorithm, the manner in which this instrument acquires its measurements is reviewed.

There are two types of calibrations: internal and external. The internal calibration measures the gain transfer function of the instrument. The gain transfer function relates the voltages at the Dicke switch to those outputted by the detection board. By measuring this function and monitoring changes in it, the final estimate of the scene brightness temperature is not affected by fluctuations in the internal system gain transfer function.

In the AOC SFMR, this is accomplished using a reference and internal calibration load that are attached to the Dicke switch. The internal calibration load for this instrument was initially a hot load (noise diode) but was replaced with a cold load (cold FET) during the 2005 season. For this reason it is referred to as the internal cold/hot load. Both this load and the reference load have a stable and known noise emission (or brightness temperature). The Dicke switch periodically selects one of these loads and the output voltage of the instrument is recorded (i.e. V_{ical} and V_{ref}). By monitoring the difference between these two voltages, changes in the internal gain transfer function can be measured and then corrected for in the processing algorithm that derives the brightness temperature of the scene.

The external calibration, which is often referred to as the calibration of the instrument, accounts for the reflective and absorptive losses in the antenna system. Before stepping through the external calibration process, it is important to understand how this system measures the scene brightness temperature.

During operation, the three voltages shown in Figure 7 are measured. Most likely a sample and hold circuit is used in the detection board such that these voltages are low pass filtered and held synchronously with the switching of the Dicke switch and then sampled by an analog to digital converter. That is, when the Dicke switch connects the antenna feed to the receive chain, the signal is amplified, down converted, filtered, and detected to produce the voltage $V_{A'}$ or its digital representation (i.e. ADC output bits). In this manner, $V_{A'}$ represents the scene emission incident on the antenna reduced by the absorptive and reflective losses of the antenna and antenna feed, plus the noise contribution of the antenna feed and antenna that comes from their losses. The summation is then multiplied by the gain transfer function of the instrument. By switching between the antenna feed, reference load and the internal cold/hot load, at rates much faster than changes in the gain transfer function, and measuring / calculating the difference signal (i.e. $V_{A'} - V_{ref}$, $V_{ical} - V_{ref}$), the effects of these gain transfer function changes are minimized and can be accounted for. Further, the noise contribution from the receiver components, such as the amplifiers, is the same irregardless of the Dicke switch position and therefore disappears in the difference. The only unknown at this stage is the absorptive and reflective losses of the antenna system. Thus, the external calibration process aims to account for these losses.

The calibration approach that we developed as part of this effort attempts to calibrate the instrument to the model function while installed on the aircraft. Taking advantage of the model function's insensitivity to low through moderate winds (< 30 kt), this approach can be automated to minimize requirements on the operator. Furthermore, this approach is designed to place minimal constraints on the mission in order that it can be performed routinely and/or as the opportunity or need arises. Note that the calibration is not expected to drift throughout the experiment season. However, the capability to periodically perform the calibration offers end users a higher level of confidence in the data.

For a Hach-Dicke mode radiometer, the scene brightness temperature (T_b), neglecting the absorptive losses of the antenna (at first), can be expressed as:

$$T_b = \left(\frac{V_A - V_{ref}}{V_{ical} - V_{ref}} \right)\left(K - T_{ref}\right) + T_{ref} \qquad (1)$$

where T_{ref} is the physical temperature of the reference load and K is the calibration coefficient. V_A, V_{ref} and V_{ical} are the detected signals shown in Figure 7. Note that this equation only contains a gain number for the calibration, and it is this feature that will enable us to derive the calibration from a single calibration

load (i.e. the ocean surface at low / moderate wind speeds). Solving for the calibration number, K can be expressed as:

$$K = \left(\frac{V_{ical} - V_{ref}}{V_A - V_{ref}} \right)\left(T_b - T_{ref} \right) + T_{ref} \qquad (2)$$

From equation (2), the only unknowns are the calibration number, K, and the scene brightness temperature, T_b. This means that if T_b is known, the calibration number can be derived directly from the measurements.

Figure 8 plots the ocean surface brightness temperature as a function of the ocean surface wind speed at 10 m altitude. The green curve is for 7.09 GHz and the red curve is for 4.74 GHz (upper and lower channels of the AOC SFMR). As this figure clearly shows, the brightness temperature is not very sensitive to the wind speed for low to moderate wind speeds (less than 30 knots). By deploying a GPS dropsonde to measure the winds or even simply extrapolating the flight level wind speed, a reasonable estimate of the brightness temperature can be made (within 0.1 Kelvin). The only other parameter value needed is the sea surface temperature (SST). Given that the SST is known (e.g. available from embedded SST maps), then under these conditions (which occur often), the brightness temperature can be estimated using the retrieval brightness temperature model. Using equation (2), the calibration coefficient can then be determined. Not only does this allow the calibration coefficient to be automatically determined during any flight, but it also automatically tunes to the model function so that any biases in the model function are immediately accounted for.
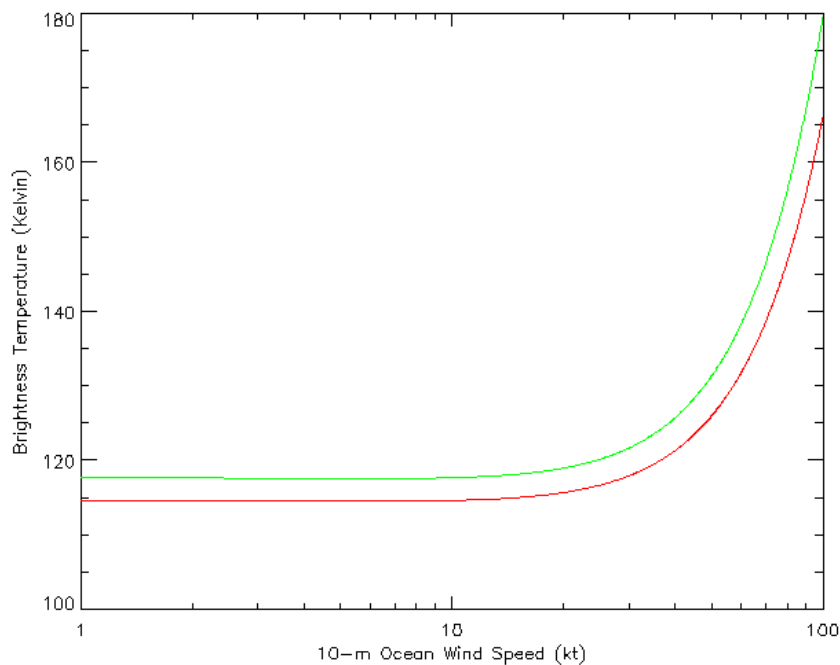

Figure 8: Ocean surface brightness temperature plotted versus 10-m wind speed (green - 7.09 GHz, red - 4.74 GHz).

To demonstrate the performance of this technique and its potential for operational use, equation (2) was applied to data obtained with the AOC SFMR during a test flight on 29 June 2005. In this case, the only information used to derive the calibration coefficient for each channel is the flight level data (i.e. altitude, flight level wind speed, flight level ambient temperature). The modeled Tb values were calculated using these flight level data and the SFMR Tb model function. No surface wind measurements were used. The SST was assumed to be 28 deg Celsius. The only filtering applied to the data was the removal of points where the pitch deviated by more than 3 degrees from the mean and the absolute value of the roll was greater than 3 degrees. Figure 9 plots the altitude, flight level wind speed and the flight level ambient temperature. During this time, the aircraft flew at several different altitudes experiencing different ambient temperatures and the flight level winds fluctuated from 2 to 7 m/s. Figure 10 plots the derived calibration number (K) for each channel. With the exception of the 5.31 GHz channel which experienced some anomalies at the beginning of this data record (potentially interference), the calibration numbers have a standard deviation of less than 2 K. In practice, averaging would be implemented and the standard deviation after averaging would be reduced by a couple orders of magnitude. Neither surface wind measurements nor SST measurements (or table) were inputted, which resulted in additional noise. Despite these factors, the numbers appear to be very stable. Furthermore, these values show no dependence on altitude / ambient air temperature or flight level wind speed. If the absorptive losses in the antenna system were significant, the measured antenna temperature (or brightness temperature) would have varied with the ambient temperature. There is no noticeable variation (correlation coefficient between the calibration number and the ambient temperature was 0.2 percent). Therefore, equation (2) is valid without needing to add in a correction for the absorptive losses.

Since there is no dependence on the flight level wind speed and the calibration numbers are essentially flat, the premise that one can use the ocean surface at low to moderate wind speeds as a calibration target seems valid. This is very significant. Currently, ProSensing, Inc. performs an elaborate laboratory calibration of the AOC SFMR. Their traditional calibration procedure results in a calibration equation with several coefficients and an offset. The offset comes from the fact that they perform a correlation analysis to relate internal temperature changes to differences in the output voltage. This process introduces an offset that otherwise should not be present. It also requires that multiple calibration targets be used to solve for both the gain and offset values. More importantly, this calibration approach does not take into account the effects of the aircraft on the reflective losses of the antenna nor any differences or biases with the model function used to retrieve the wind and rain from the SFMR measurements. The approach proposed here can be implemented with virtually no impact to operations, would essentially cost nothing to perform, can be performed during almost any flight since low to moderate wind speeds are almost

always encountered and provides a true calibration of the instrument to the model function.

This approach was presented at the 2006 Interdepartmental Hurricane Conference (IHC). Initial discussions with the Air Force, NOAA AOC and NOAA HRD were positive. However, further discussions between NOAA and ProSensing lead to this approach not being selected for implementation for the 2006 hurricane season. If the JHT program desires this approach to be further evaluated, the JHT SFMR team will apply this technique to the 2005 and 2006 data sets following the 2006 hurricane season and present the results in a separate report prior to the beginning of the 2007 hurricane season.

3.1.3 Calibration / Validation Tool

With the decision to calibrate the AOC SFMR instrument in a similar manner to previous years, the JHT SFMR team switched gears to develop an operational tool to validate the calibration. As a quick review, the current calibration approach selected by NOAA AOC is as follows:

Step1: The AOC SFMR units are shipped to ProSensing's facilities. At their location, engineers and technicians perform a radiometric calibration to relate the SFMR measurements to scene brightness temperature values. The details of this calibration procedure are proprietary to ProSensing, thus cannot be discussed here. ProSensing provides a table of coefficients that are used by a transfer function that produces brightness temperature measurements from the SFMR radiometric and internal temperature measurements. The instrument is then shipped back to AOC and installed on the aircraft.

Step 2: A "calibration" flight is executed where the SFMR is flown over the ocean under low to moderate ocean surface wind conditions and clear sky. Recall from Figure 8 that under such conditions, the brightness temperature measurements will be fairly insensitive to small fluctuations in the wind speed making it easier to estimate the brightness temperature of the ocean surface. The flight pattern is executed at multiple altitudes and a NOAA buoy is over flown in order to gather coincident, *in situ* ocean surface wind measurements. The *in situ* ocean surface wind measurements (GPS dropsondes could be used as well) are compared with the SFMR retrievals. The retrievals are derived from the brightness temperature measurements produced using ProSensing's calibration coefficients derived during step 1. Using the geophysical model function (GMF), the wind measurements are translated to brightness temperature estimates, and the offset between these and the SFMR measurements are calculated. The calculated offsets are applied to the SFMR transfer function, and the retrieved winds are again compared with the *in situ* winds. Once in agreement, the final offset values are published and used for the duration of the season provided the instrument is not removed from the aircraft. Note that for the 2006 calibration flight, an additional altitude correction factor was calculated and incorporated in the final calibration transfer function.

Note that in this procedure, only the ocean surface wind speed is considered. That is, the rain retrieval is ignored. Although the flights are executed under clear sky conditions, the rain estimates will have a certain statistical behavior that can be easily measured and used to ensure the tuning process is tuning both to the wind speed and to the rain rate dependence of the GMF. To better understand this, the behavior of the retrieval process is described below.

Using the simulator described earlier, three parameters were calculated for the clear sky case: the mean rain rate, the standard deviation of the rain rate estimates and the zero hit percentage of the rain rate estimates. Note that the zero hit percentage is the percentage of rain rate estimates that were equal to 0 mm/hr for a given wind speed. Since the SFMR brightness temperature measurements are noisy, non-zero rain rate estimates can occur when rain is not present. The SFMR retrieval process sets these values to 0 mm/hr threshold, in other words, it does not allow for negative rain rates (this is an oversimplification to describe the outcome in a straightforward manner). Thus, the zero values actually represent negative rain rate values.

Using the simulator, the dependence of the three parameters described above on ocean surface wind speed and ΔT was calculated. Figure 11 through Figure 13 plot these values for wind speeds from 0 to 10 m/s and ΔT values from 0.05 K to 1 K.   All three parameters exhibit no dependence on wind speed for the range shown. The zero hit percentage shows no dependence on the measurement precision (i.e. ΔT), while the mean and standard deviation of the rain rate estimates increase along with ΔT. This is in accordance with expectations. The noise has a zero mean Gaussian distribution. Thus, the rain retrievals should be negative half of the time and positive half of the time. Since the retrieval process forces the rain retrievals to be zero or higher, half of the retrieved values are zero and the mean retrieved rain rate has a non-zero value. The larger the ΔT, the larger the mean (or bias) in the rain rate and the larger the standard deviation in the rain rate retrievals.

To evaluate this over the full range of wind conditions, the simulator was run for wind speeds from 0 to 80 m/s in 5 m/s steps and at several different ΔT values. Note that the reported ΔT of the AOC SFMR at the time of this work was 0.17 K for a 1 second integration time. This translates roughly to 0.2 K for the sampling strategy implemented by the AOC SFMR. Figure 14 through Figure 16 plot the results. Recently it was determined that the actual ΔT is 0.5 K. This does not affect the conclusions however. Once again the zero hit percentage is independent of wind speed and ΔT. The mean and standard deviation of the rain rate retrieval increase with wind speed above approximately 25 m/s and increase with ΔT as expected. The increase with wind speed occurs at a point in GMF where the sensitivity of the brightness temperature on wind speed begins to increase and as a result the retrieval process assigns the small variations in the measurements to rain rather than wind speed.
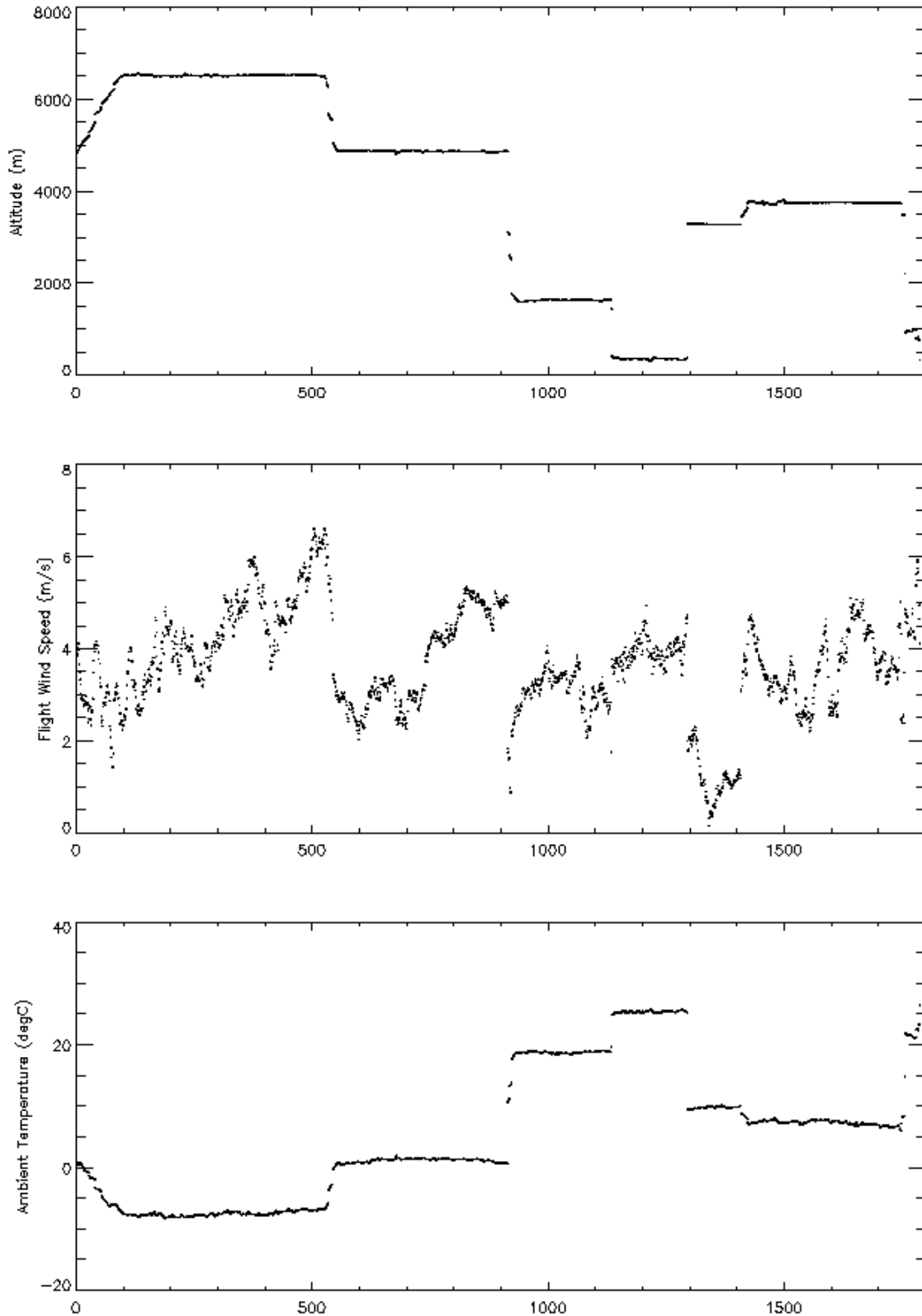
Figure 9: The altitude, flight level wind speed and ambient air temperature for the mission on 29 June 2006 are plotted.
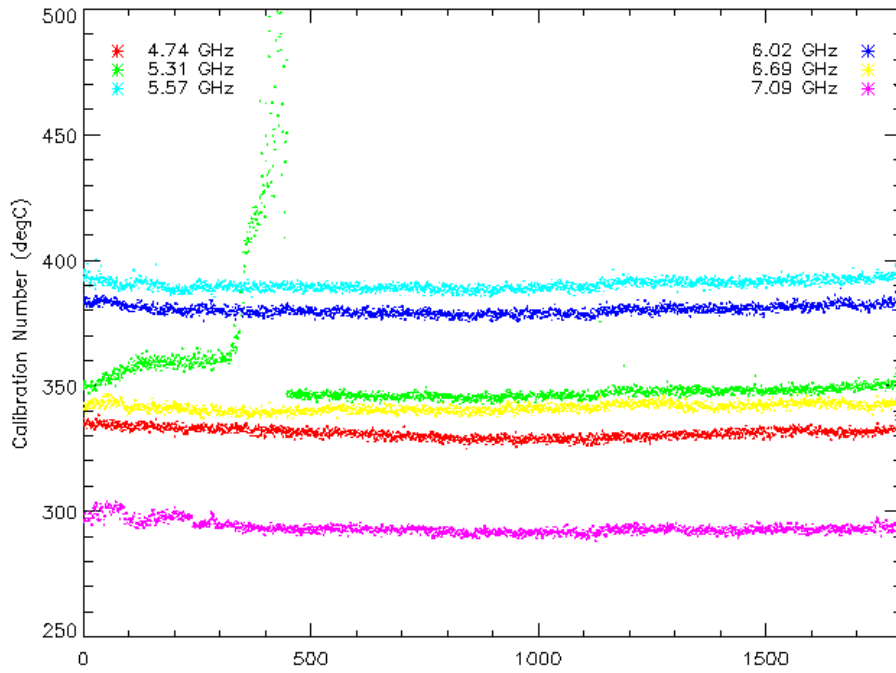
Figure 10: AOC SFMR calibration numbers (*K*) derived from the raw data on 29 June 2005 using the auto calibration procedure.
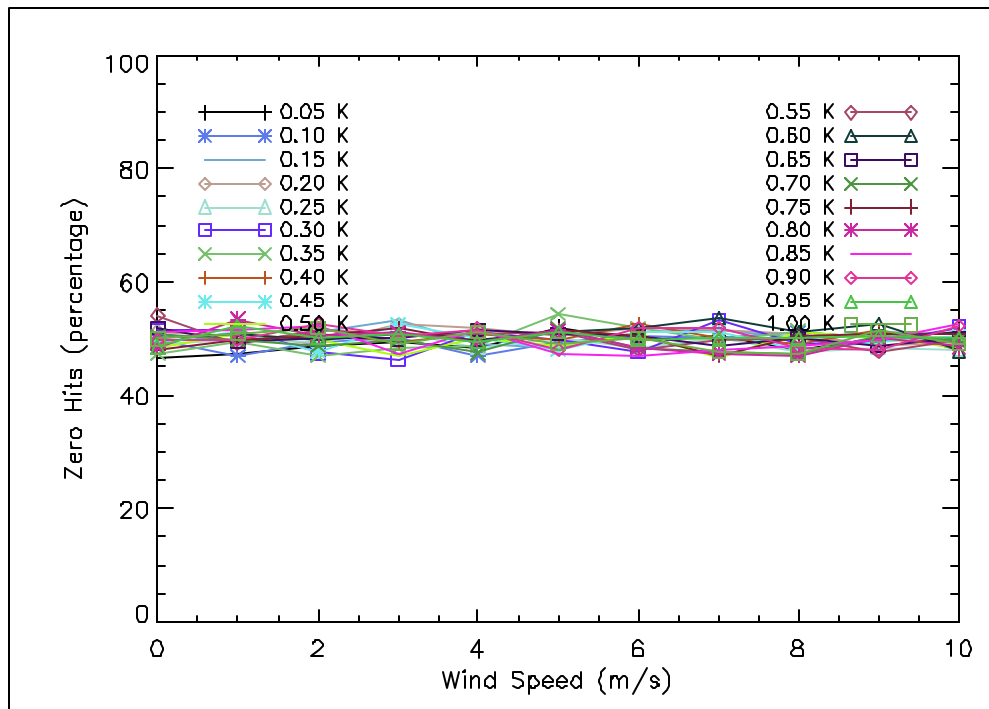

Figure 11: Percentage of rain rate estimates equal to 0 mm/hr plotted versus wind speed and color coded by the DT of the measurements (actual rain rate = 0 mm/hr).
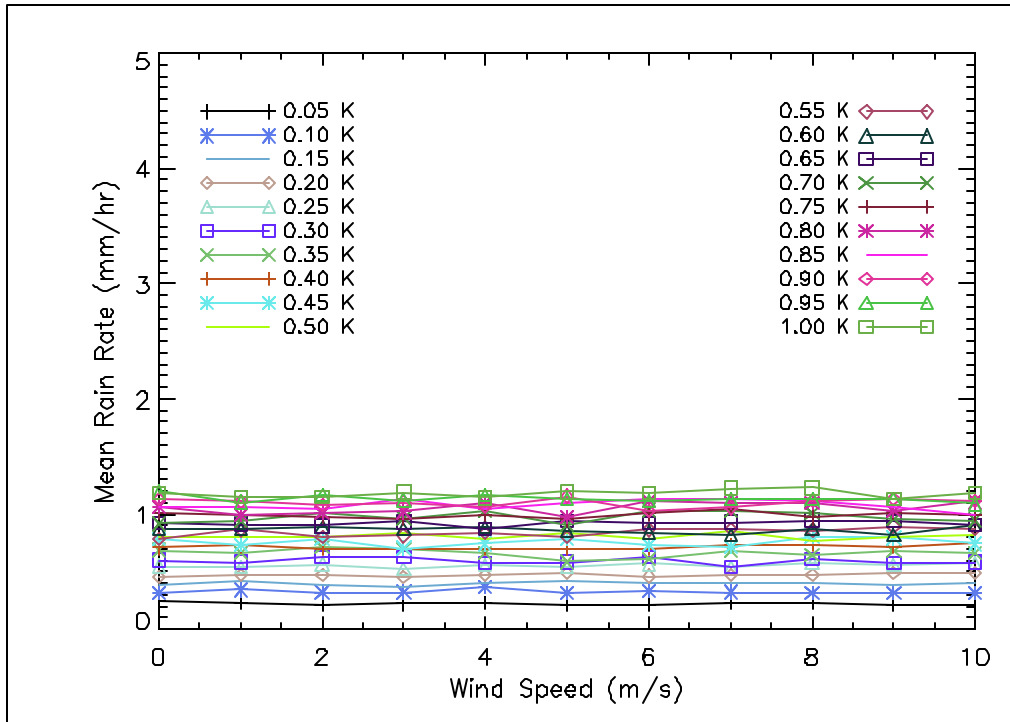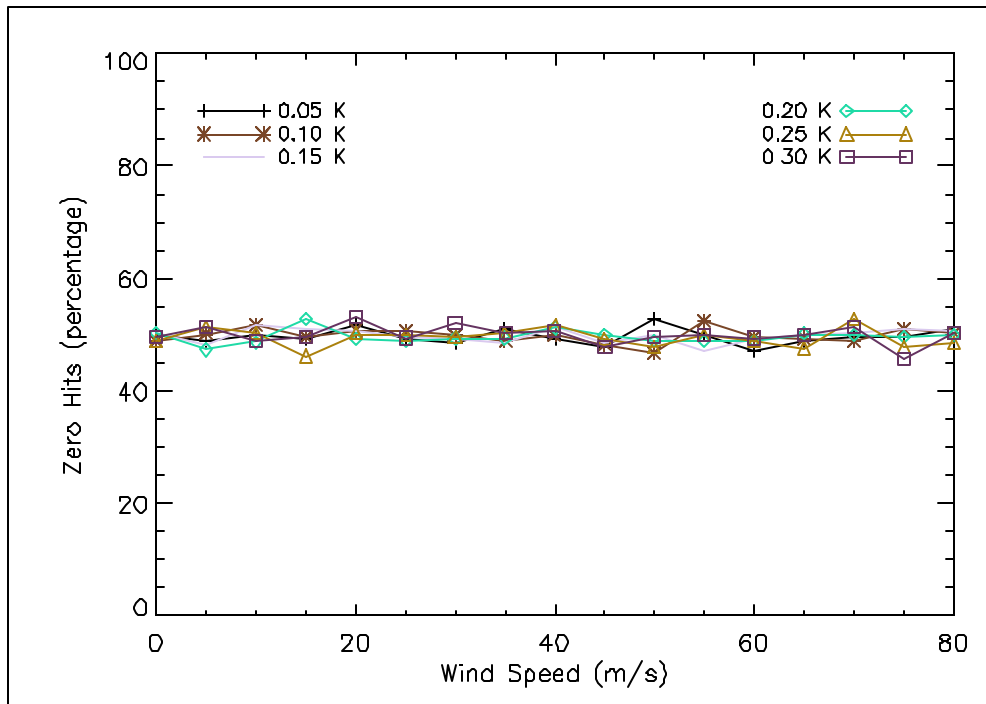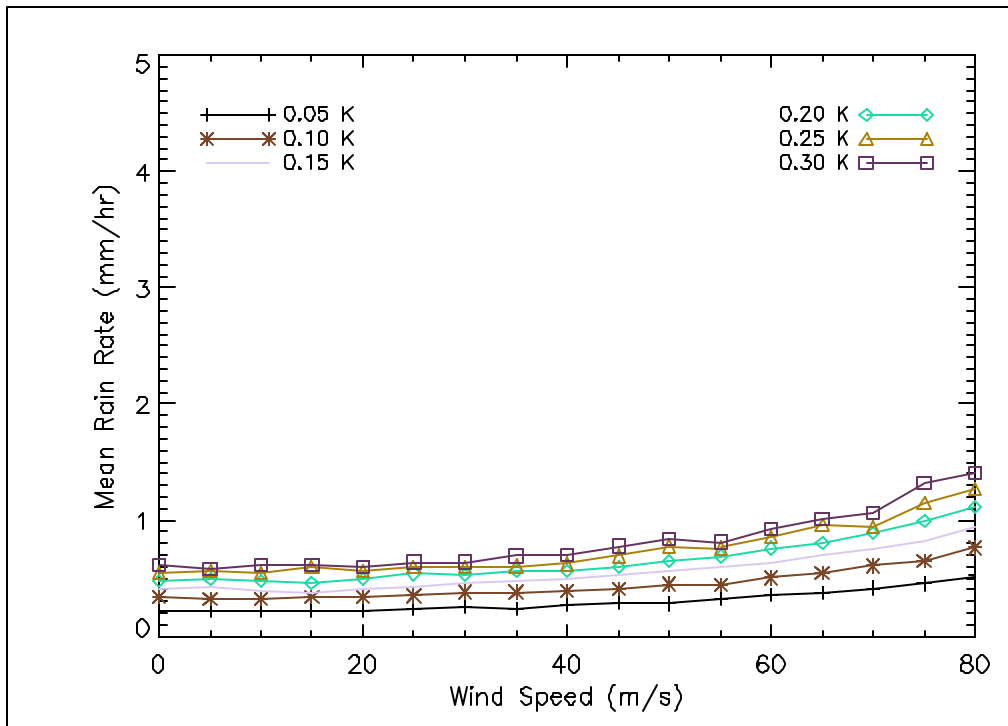
Figure 12: Mean retrieved rain rate plotted versus wind speed and color coded by the DT of the measurements.
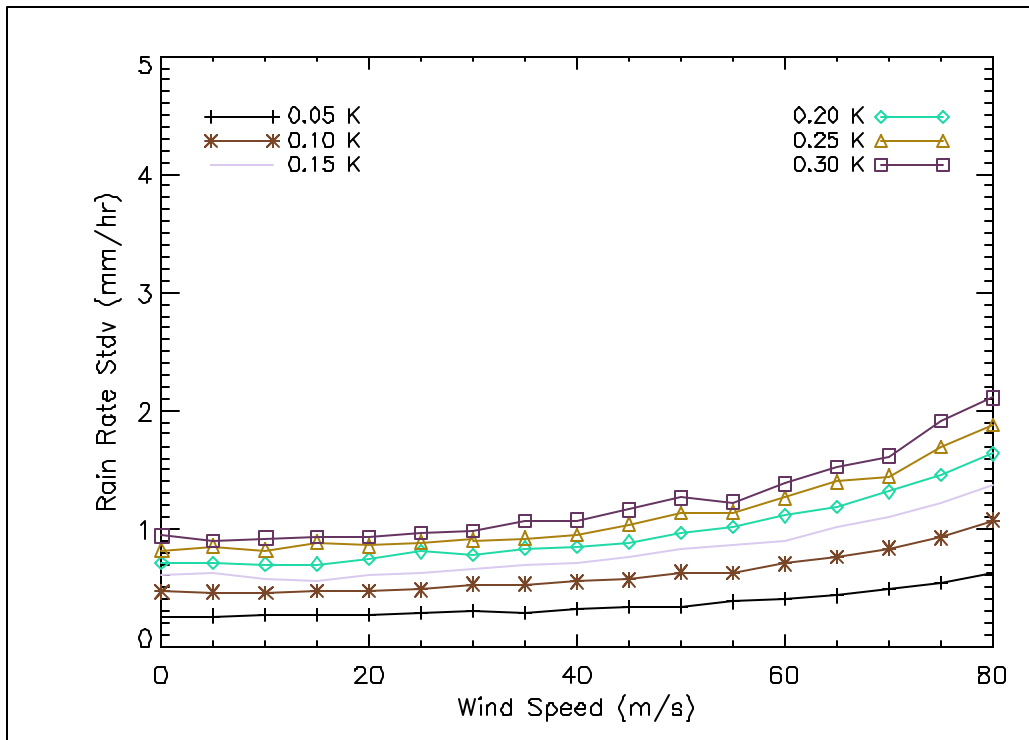

Figure 13: Standard deviation of the retrieved rain rate plotted versus wind speed and color coded by the DT of the measurements (actual rain rate = 0 mm/hr).

Figure 14: Percentage of rain rate estimates equal to 0 mm/hr plotted versus wind speed and color coded by the $\text{D}T$ of the measurements (actual rain rate = 0 mm/hr).

Figure 15: Mean retrieved rain rate plotted versus wind speed and color coded by the $\text{D}T$ of the measurements (actual rain rate = 0 mm/hr).

Figure 16: Standard deviation of the retrieved rain rate plotted versus wind speed and color coded by the ΔT of the measurements (actual rain rate = 0 mm/hr).

Now consider the impact of a calibration error on the zero hit percentage parameter. Two cases are shown: 1) a positive 0.2 K bias and 2) a negative 0.2 K bias are introduced to the highest frequency channel. Recall the 0.2 K is the requirement to keep the maximum possible absolute mean error in the wind retrieval to less than 1 knot. Figure 17 and Figure 18 plot the zero hit percentage parameter as a function of wind speed and ΔT for these two cases. With a positive bias, the zero hit percentage decreases and with the negative bias it increases. This is because the bias introduces a larger / smaller spread in the measurements with respect to frequency and thus results in higher / lower rain rate retrievals. As the ΔT increases, the zero hit percentage moves towards 50 percent because the actual retrieval becomes more noisy resulting in more zero (or negative) solutions. Nevertheless, even with this very small bias, the zero hit percentage parameter shows clearly that the measurements do not agree with the model function and the calibration needs to be tuned. By simply monitoring the percentage of retrievals that are 0 mm/hr in rain free conditions (wind speed does not matter), it can be determined whether the SFMR is properly calibrated. This simple method does not require any information except for the rain rate estimates which are readily available on the NOAA WP-3D aircraft and will be available on the 53rd Air Force Reserve WC-130 aircraft. In fact, the tool could even be implemented on the ground using the real-time retrieval estimates that are sent to NHC. Alan Goldstein of NOAA AOC has been briefed on this approach. He is now using it to help tune the final AOC SFMR calibration numbers for the 2006 hurricane season.
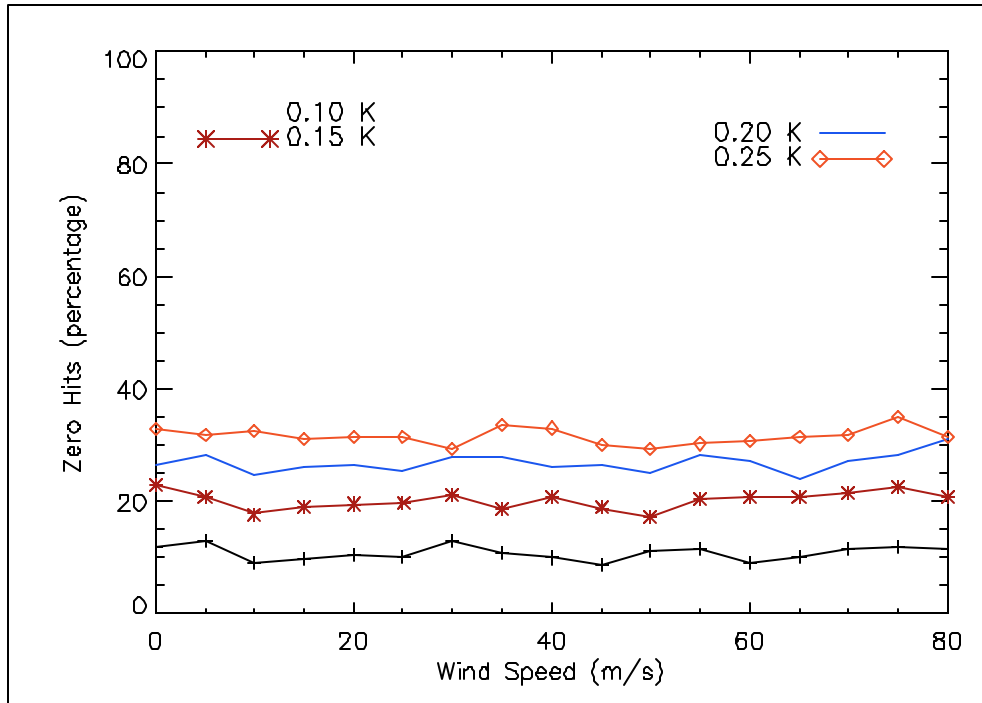
Figure 17: Percentage of rain rate estimates equal to 0 mm/hr plotted versus wind speed and color coded by the DT of the measurements (actual rain rate = 0 mm/hr, Tb measurements at the highest frequency channel have a 0.2K bias).
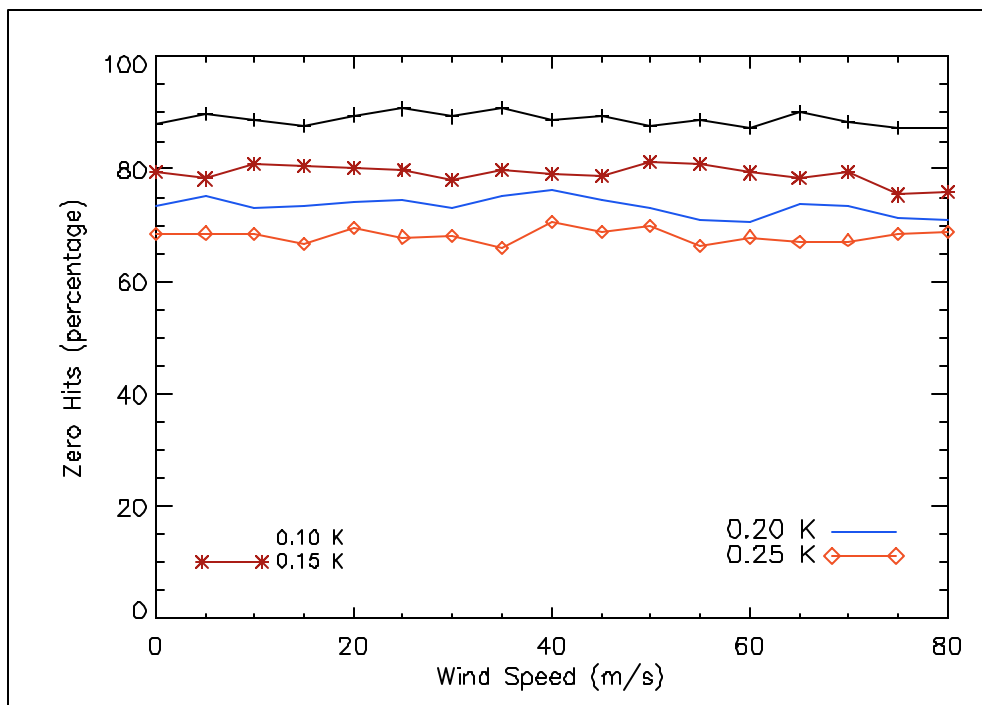

Figure 18: Percentage of rain rate estimates equal to 0 mm/hr plotted versus wind speed and color coded by the DT of the measurements (actual rain rate = 0 mm/hr, Tb measurements at the highest frequency channel have a -0.2K bias).

3.2 Sea Surface Temperature

The ocean surface brightness temperature depends on the SST, and thus, errors in our knowledge of the SST could negatively impact the accuracy of the SFMR near ocean surface wind speed estimates. To date, the real-time SFMR retrieval processor has used a static SST value that is manually entered (nominally 28 deg C). The AOC SFMR real-time processor, which is now deployed on the NOAA WP-3D aircraft and that will be used on the 53rd Air Force Reserve WC-130 aircraft, has the capability to automatically ingest SST values through a latitude-longitude SST table. Before implementing such a procedure operationally, the JHT SFMR team has focused on: 1) determining the accuracy requirement for SST estimates and 2) surveying the available SST products that could serve as a candidate to provide the SST tables.

In order to determine the required accuracy for the SST estimates, the impact of SST errors on the SFMR retrieval accuracy was evaluated. Using the SFMR retrieval simulator, the brightness temperature measurements for all combinations of 7 different wind speeds (33, 50, 64, 83, 96, 114, and 135 knots) and 5 different rain rates (0, 5, 10, 20, 30 and 40 mm/hr) were calculated. For each wind speed and rain rate combination, 1000 independent realizations were created with a ΔT of 0.5 K for each frequency channel. The simulated measurements were passed to the retrieval processor and the wind speed and rates derived. This process was repeated as the SST input to the retrieval processor was cycled over a range of +/- 5 deg C in 1 deg C steps. For each SST, wind speed and rain rate, the mean error and standard deviations of the retrievals were calculated.

Figure 19 presents the results. In the upper and lower left panels the mean error and standard deviation of the wind speed retrievals are plotted versus the SST error and color coded by wind speed. The values have not been stratified with respect to rain rate because neither the mean error nor standard deviation of the wind speed retrievals exhibits any dependence on rain rate for a given SST error. The reason is fairly simple. The SST only affects the ocean surface brightness temperature, and the GMF can adequately account for this effect by adding or subtracting from the wind speed. Because the ocean surface brightness temperature has a small dependence on frequency, an SST error produces a slight different change in the predicted brightness temperature for each frequency. This is unlike the calibration errors discussed in the previous section that cause a shift in the brightness temperature measurements that do not adhere to the frequency dependence as modeled by the GMF. This is further supported by the upper and lower right panels that plot the mean error and standard deviation of the rain rate retrievals as a function of SST error. As these two plots show, the rain rate retrievals are not significantly affected by SST errors. Once again this is consistent with the explanation discussed above.
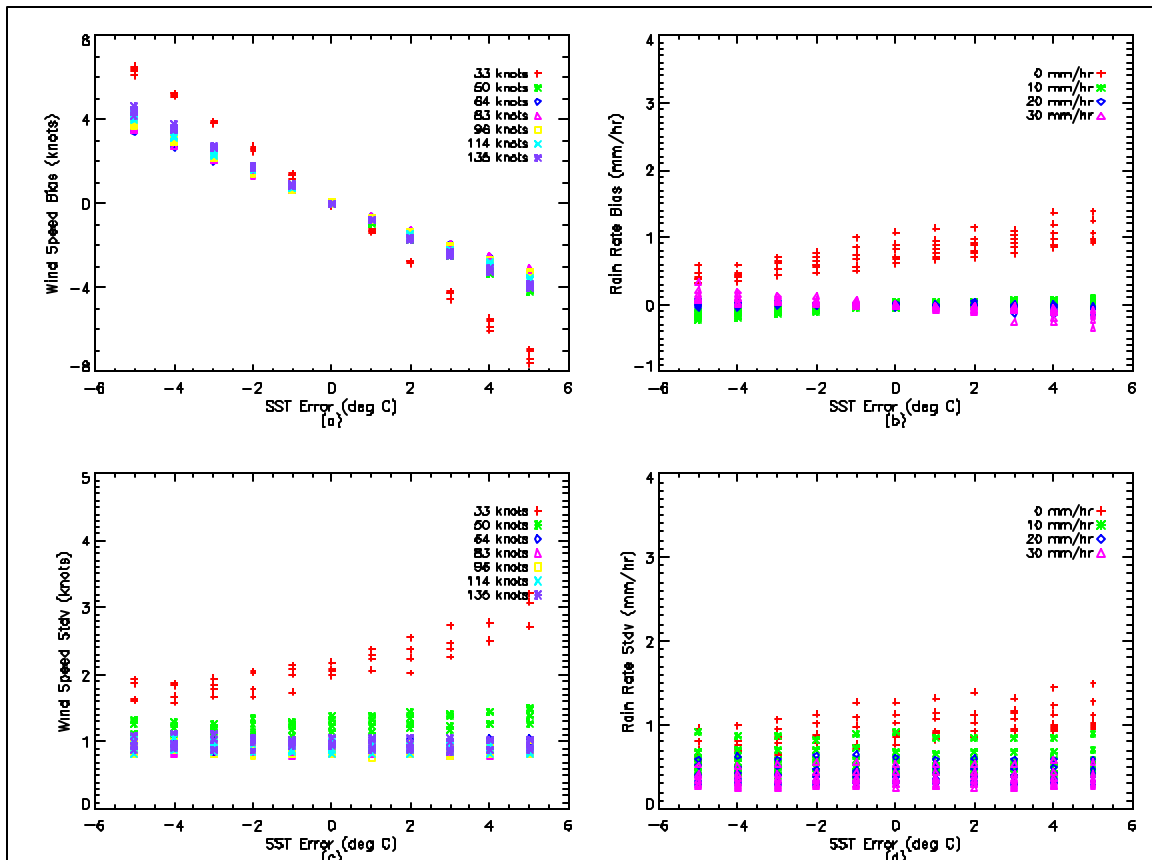
Figure 19: SST error effects on the wind speed and rain rate mean errors and standard deviation.

For wind speeds at or above storm force, the mean wind speed error caused by an SST error is linearly related to the SST error (slope is approximately 1 knot / 1 deg C). This linear relationship is the result of two things: 1) rain rate does not play a role, and 2) the excess emissivity is linearly related to wind speed at hurricane force winds. For winds less than storm force, the excess emissivity has a quadratic relationship with wind speed and its sensitivity decreases with wind speed. Thus, small SST errors can introduce large biases in the wind speed estimates. Finally, the standard deviation of the wind speed retrievals seems to be invariant with SST errors for hurricane force winds, and for winds below storm force, the standard deviation of the wind speed increases with increasing SST error.

Focusing on hurricane force winds, the SST must be known to within approximately 1 deg C to ensure that the error introduced into the retrieval process is less than 1 knot. To accomplish this task for all conditions and locations, a method to retrieve the SST from the SFMR instrument is required. NOAA NESDIS and RSS are working on different approaches but still have not found a solution given the current instrument's capabilities. This will be an effort that will continue in the second year of the JHT. In the mean time, SST values can be retrieved from satellite sensors and/or models, but these will have

limitations. Most techniques for measuring the SST either cannot penetrate clouds and rain or do not provide the required spatial sampling and accuracy.

Table 2 presents potential sources for global SST estimates. GOES provides the highest temporal resolution and adequate spatial resolution but cannot provide complete spatial coverage because it cannot see through clouds. POES provides reasonable estimates as well but also cannot provide the necessary spatial / temporal coverage. The other products either cannot provide adequate sampling or resolution or are modeled fields rather than measured. Nevertheless, a combination of these measurements can serve to at least improve the current situation where no SST information is being provided.

Table 2: Potential Sources for Global SST

Product	Coverage	Spatial	Temporal	Accuracy	Availability
GOES Retrieved SST	180W to 30W, 45S to 60N	5km	Hourly	Mean: 0.2 RMS: 0.7	FTP (NOAA) or direct
POES Retrieved SST	Global	1km	Twice Daily per satellite	Mean: 0.1 RMS: 0.5	FTP (NOAA) or direct
TMI Retrieved SST	Global, 40S to 40N	50km	Twice Daily	Mean: 0.1 RMS: 0.7	FTP (Remote Sensing Systems)
WindSat Retrieved SST	Global	50km	Twice Daily	Mean: 0.1 RMS: 0.8	FTP (NOAA) or direct
OSTIA Analyzed SST	Global	5km	Daily	Mean: 0.05 RMS: 0.5	FTP (UK Met Office)
RTG Analysis SST	Global	50km	Daily	Mean: 0.1 RMS: 0.6	FTP (NOAA)
Reynolds OI SST Climatology	Global	100km	Monthly	N/A	FTP(NOAA)

3.3   Rain Model Errors

The SFMR rain rates are basically derived from microwave attenuation, which has long been shown to be correlated with rain. With six frequencies in the range of 4.74 to 7.09 GHz, an inversion technique is used to derive only two parameters: near ocean surface wind speed and column averaged rain rate from the six available brightness temperatures. Rain attenuates differently at the six frequencies. Assuming that the radiative process is Rayleigh (which translates into a raindrop diameter requirement of less than approximately 6 mm at these frequencies), the absorption dominants over the scattering effects. A forward radiative transfer model is thereby derived by modeling an absorptive only process from rain. From this physical model, which relates the attenuation coefficient to the measurements of the brightness temperature at the six frequencies, a set of equations over-determinates the problem and therefore allows the rain rate to be estimated. The SFMR algorithm uses a power law to relate the rain rate R_r to the attenuation coefficient, $K = aR_r^b$, where the parameter

a is function of the rain rate and the frequency f, given as $a = c \ \ f^{\,n(R_r)}$, where c is a constant and $n(R_r)$ is the atmosphere's refractive index, and also a function of the rain rate.

The SFMR rain rate retrieval process is susceptible to three main sources errors: 1) errors in the model function employed; 2) differences in the observed drop-size distributions, particularly associated to differences in convective and stratiform regimes; and 3) non-uniform beam filling within the instrument's field of view. The Imaging Wind and Rain Airborne Profiler (IWRAP) can be used to derive an improved SFMR rain rate model. IWRAP flew in 2005 alongside the AOC SFMR and will do so in 2006 as well.

IWRAP measures the volume reflectivity from precipitation simultaneously at two electromagnetic wavelengths: a long wavelength that is basically not attenuated (C-band), and a shorter wavelength that is attenuated (Ku-band). The measurements of reflectivity at C-band can be matched against the retrieved SFMR rain rate retrievals to derive an empirical Z-R relationship.

Figure 20 shows such scatter plot, from measurements acquired during four consecutive flights through Hurricane Isabel (2003), together with several of the available models. Although it has been repeatedly shown in the literature that no single Z-R relationship exists due to the variations in the drop-size distribution (and this fact can be observed by the large scatter present in the plot, which is not the result of variance in the reflectivity measurements since each point is the result of averaging more than 200 independent samples), it is clear from these results that none of the relationships available in the literature follows the trend given by the SFMR –clearly indicating a problem in the SFMR rain rate model function. After applying a linear relationship to derive new rainfall rate retrievals, the SFMR observations now follow the general trend of the other models.
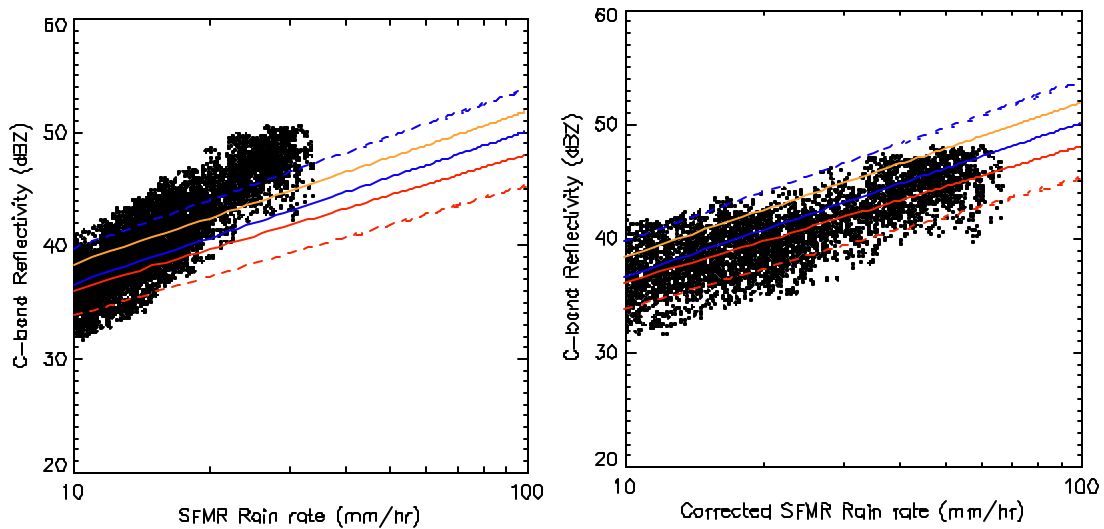
Figure 20: The left scatter plot of flight-level reflectivity measurements at C-Band and 30 degrees incidence obtained during four flights through hurricane Isabel (2003) versus the collocated SFMR rainfall rate estimates. The Jorgensen Z-R model (orange solid line), the Marshall-Palmer model (blue solid line), the NEXRAD model (red solid line), the Jones model (blue dashed line) and the Atlas model (read dashed line) are also overlaid. The right figure shows the same scatter plot where the SFMR rain rate retrievals have been corrected with a linear relationship. The same models are also overlaid.

The IWRAP dual-wavelength measurements can also be used to improve the current SFMR model functions. The differential attenuation dual-wavelength radar method uses these measurements to calculate a path-averaged specific attenuation over a given range,

$$K_S = \frac{1}{2(R_2 - R_1)} \ln\left[\frac{Z_C(R_1) \cdot Z_{KU}(R_2)}{Z_C(R_2) \cdot Z_{KU}(R_1)}\right], \qquad (3)$$

where R_1 and R_2 are the two range distances over which the attenuation is derived. The derived attenuation can be related to the rain fall rate by means of a power law (k-R model). Different path lengths in between the IWRAP reflectivity observations can be used as to extend the dynamic range of the model and retrieval. In the presence of lower rainfall rates, larger attenuations can be integrated over longer paths and higher to extreme rain rates can be retrieved using the attenuation observed within a few range gates. The greatest virtue of this dual-frequency technique is that since it is based upon the ratio of reflectivities, it is independent of calibration, and typical limitations associated with the amount of attenuation required to generate an accurate model do not apply in this situation, where attenuations in excess of 10 dB per km are commonly present.
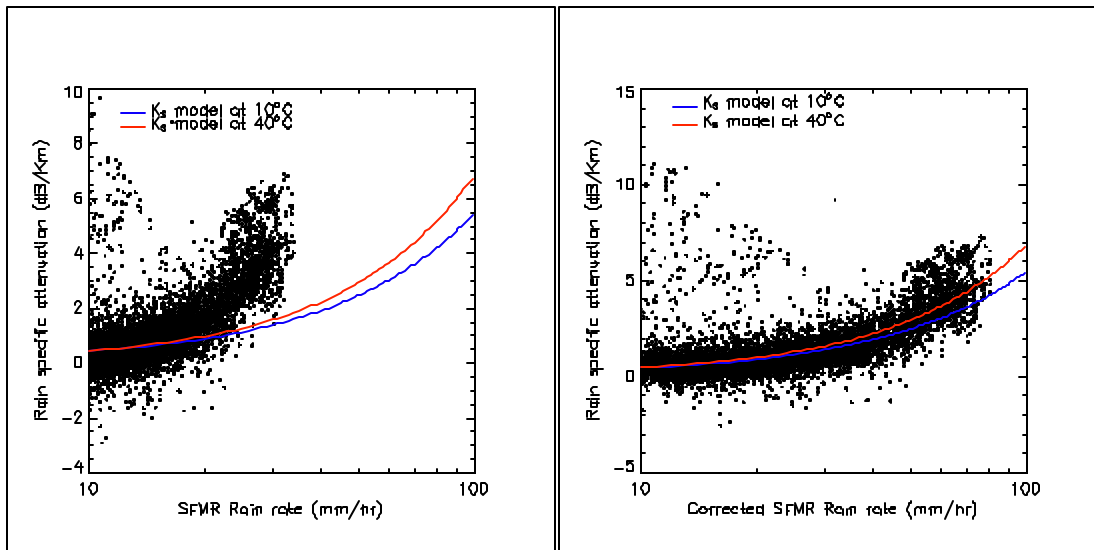
Figure 21: The specific attenuation derived from IWRP measurements is plotted versus the uncorrected and correct SFFMR rain rate retrievals.
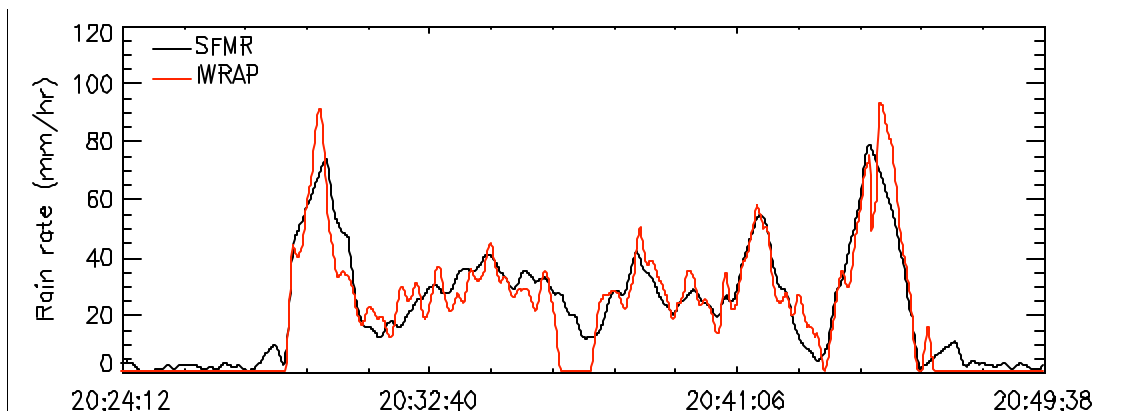

Figure 22: IWRAP rainfall rate estimates using the derived k-R model. The SFMR rainfall rate estimates are also plotted. This corresponds to an eye-wall penetration through hurricane Isabel on September 12th, 2003.

To substantiate the feasibility of the proposed approach, Figure 27 presents a scatter plot of the specific attenuation versus the SFMR rainfall rate estimates; two models derived by Atlas and Ulbrich at 10 C and 40 C are overlaid. These results are preliminary and aim mainly to illustrate the methodology and demonstrate the feasibility of the method, but should not be used to derive conclusions of the attainable performance. From the measurements shown, a power law relating the specific attenuation and the SFMR rate was derived. This relationship was then used to obtain rain rate estimates from the difference in the dual-wavelength IWRAP reflectivity measurements at flight level and 1 km range distance. Figure 28 presents an instance of such retrieval corresponding to a

flight through Hurricane Isabel (2003), showing an excellent agreement with the (corrected) SFMR rainfall rate estimates.

Although rain rate is a secondary product at this stage, the errors in the rain model that is embedded in the SFMR GMF can negatively impact the near ocean surface wind retrievals as well. To evaluate to what extent this occurs, the SFMR retrieval simulator was used once again. The different parameters of the rain model were adjusted up by -10, -5, 5 and 10 percent and the brightness temperature measurements were simulated. Then using the current model function, the near ocean surface wind speed and column averaged rain rate were derived. Figure 23 and Figure 24 plot the mean error and standard deviation of the rain rate and wind speed estimates as a function of the rain multiplier error (note rain multiplier is the constant, c, mentioned above), respectively. The mean error in the rain rate retrieval both increases as this parameter is over estimated and with rising rain rates. It is constant with wind speed. The standard deviation remains essentially constant compared to the zero error case for each rain rate. The mean error in the wind speed retrieval has the opposite effect in that it becomes more negative as this parameter is over estimated. It also depends on the wind speed and the effect worsens as the rain rate increases.

Figure 25 through Figure 28 show similar trends when the rain exponent and the frequency-rain exponent (refractive index) are under or over estimated. Note that the wind errors are not quite as large. Nevertheless, errors in the rain model cause significant mean errors in the wind speed retrievals, and thus the SFMR rain model must be updated and the new model verified.
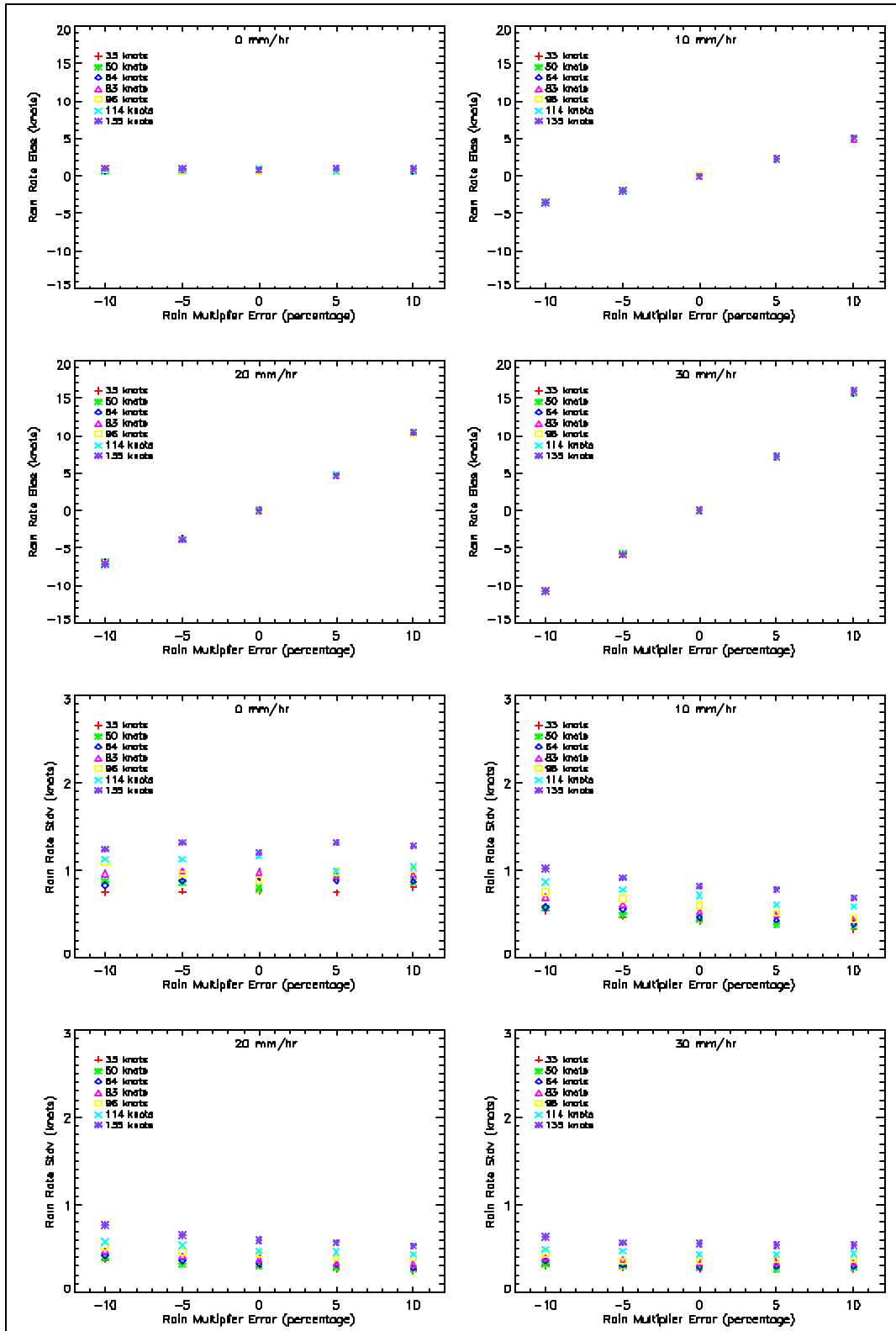
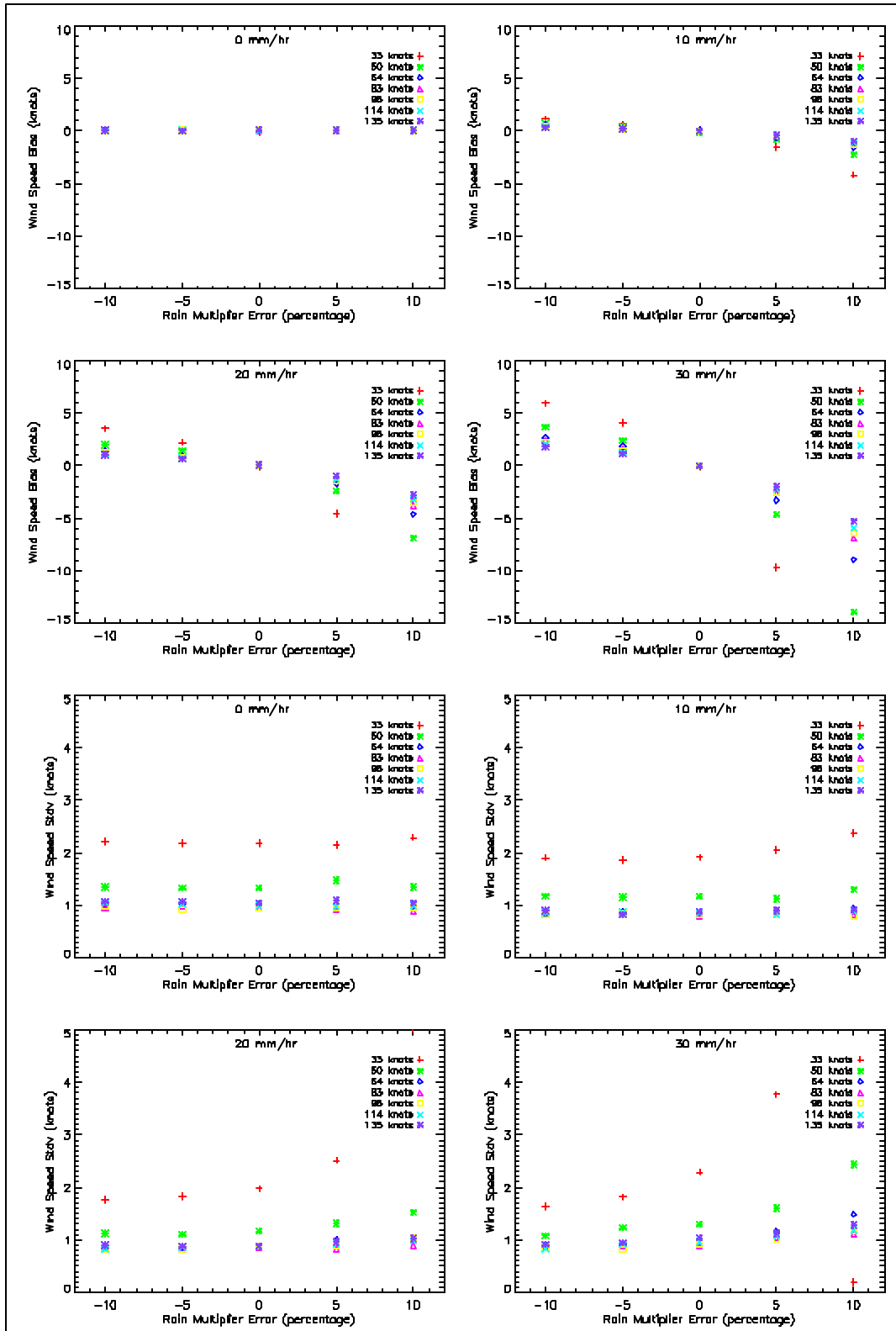**Figure 23: Error in rain retrievals caused by errors in rain multiplier factor in the rain model.**

Figure 24: Errors in the wind retrievals caused by errors in rain multiplier factor in the rain model.
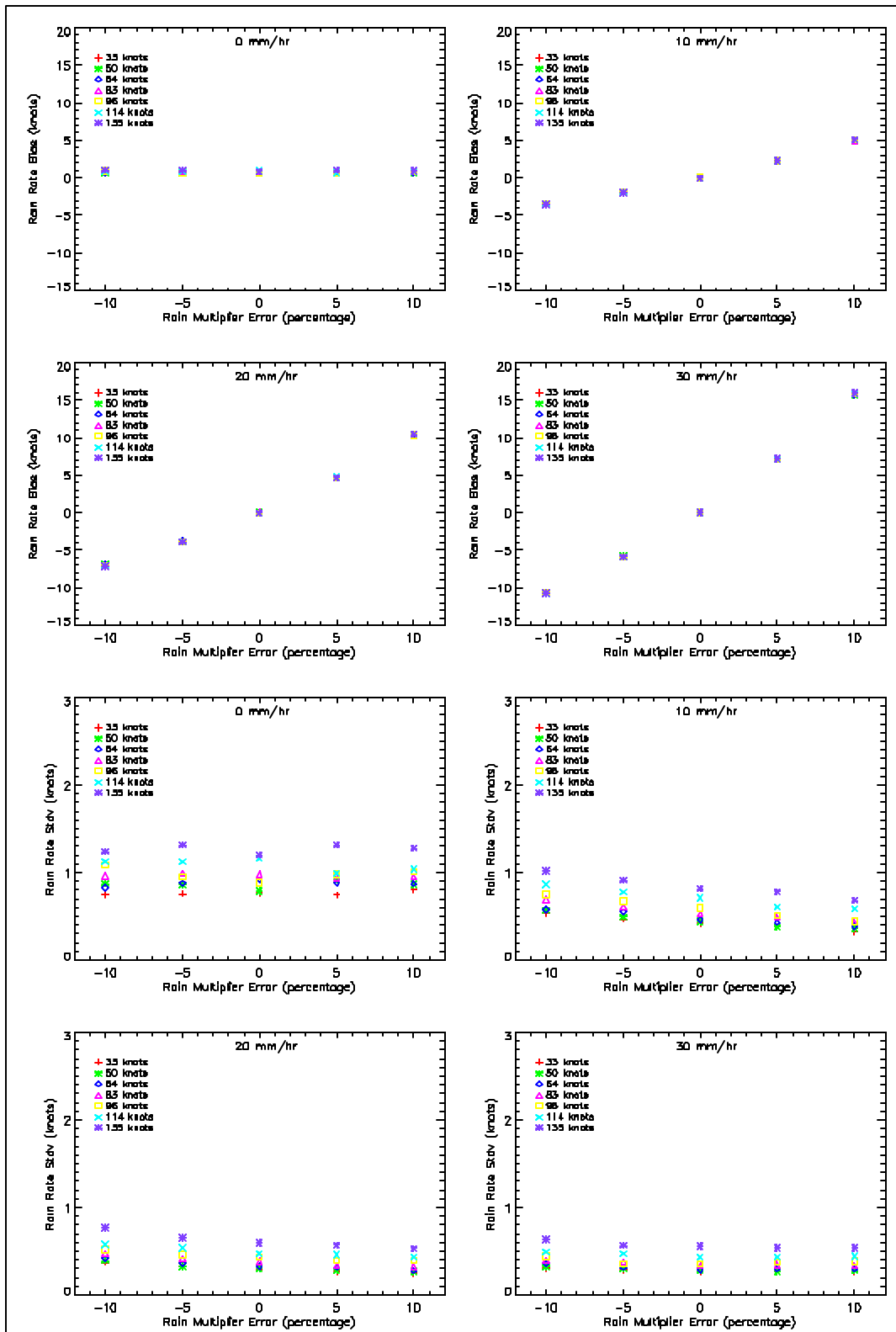
Figure 25: Errors in the rain retrievals caused by errors in rain exponential coefficient in the rain model.
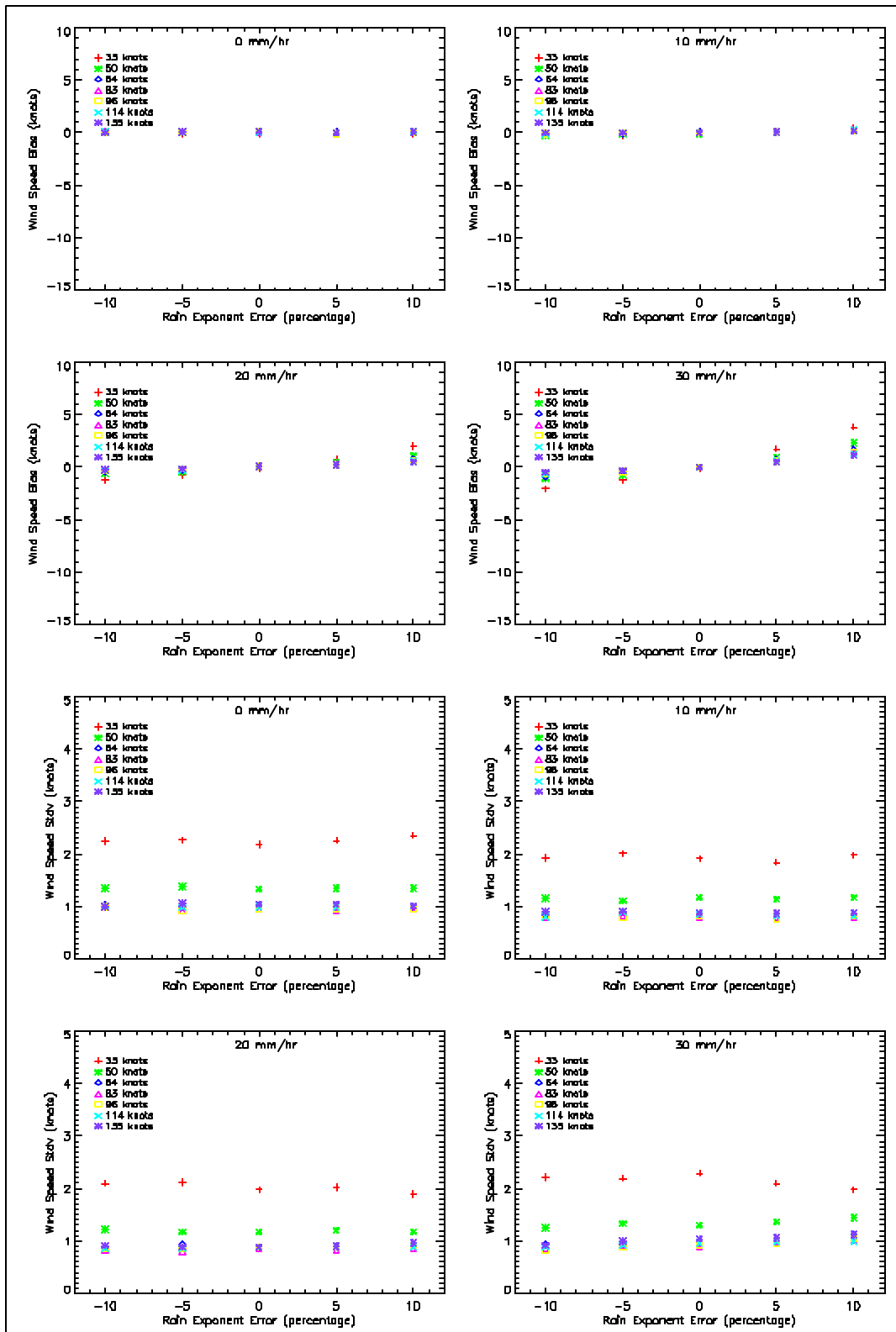
Figure 26: Errors in the wind retrievals caused by errors in rain exponential coefficient in the rain model.
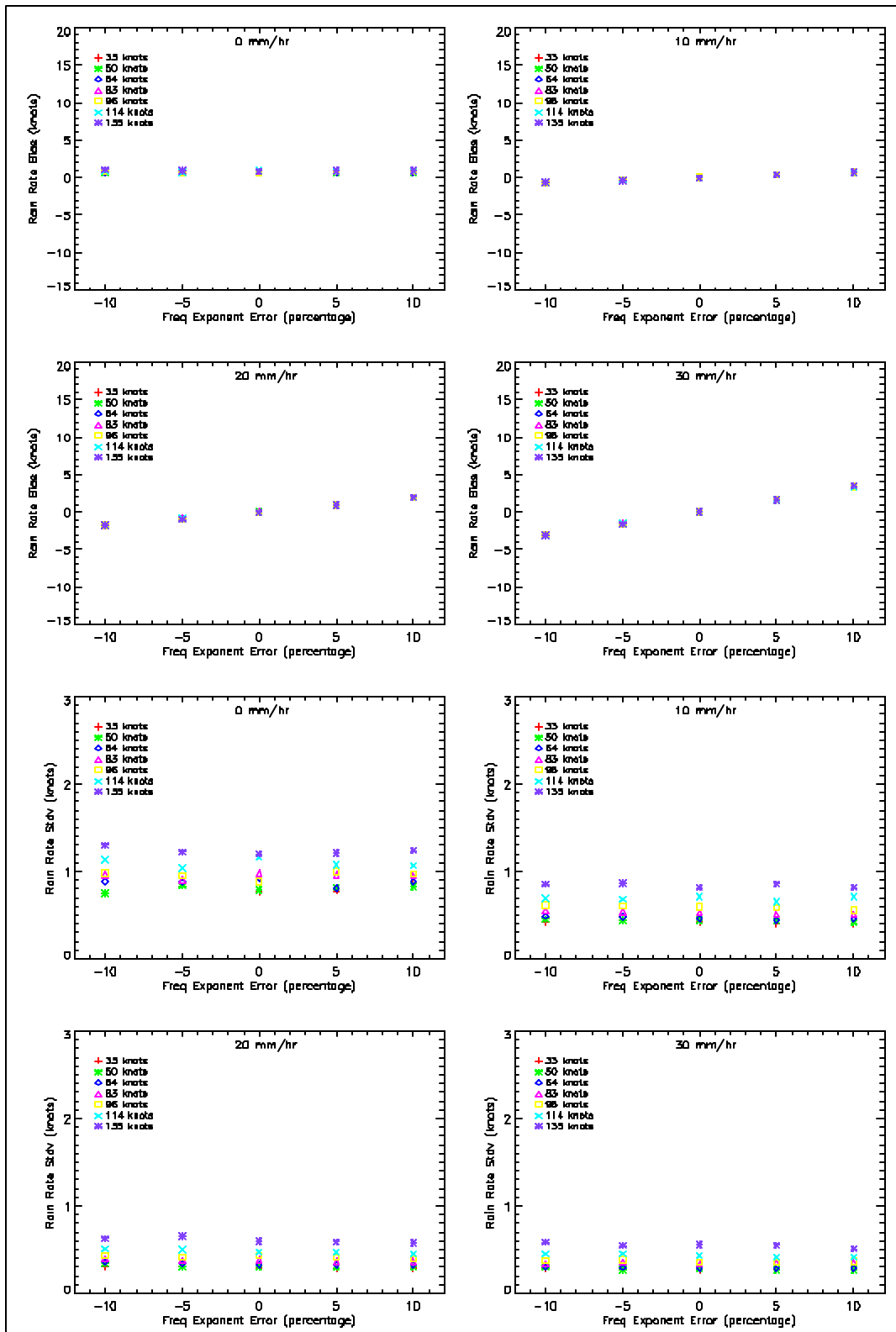
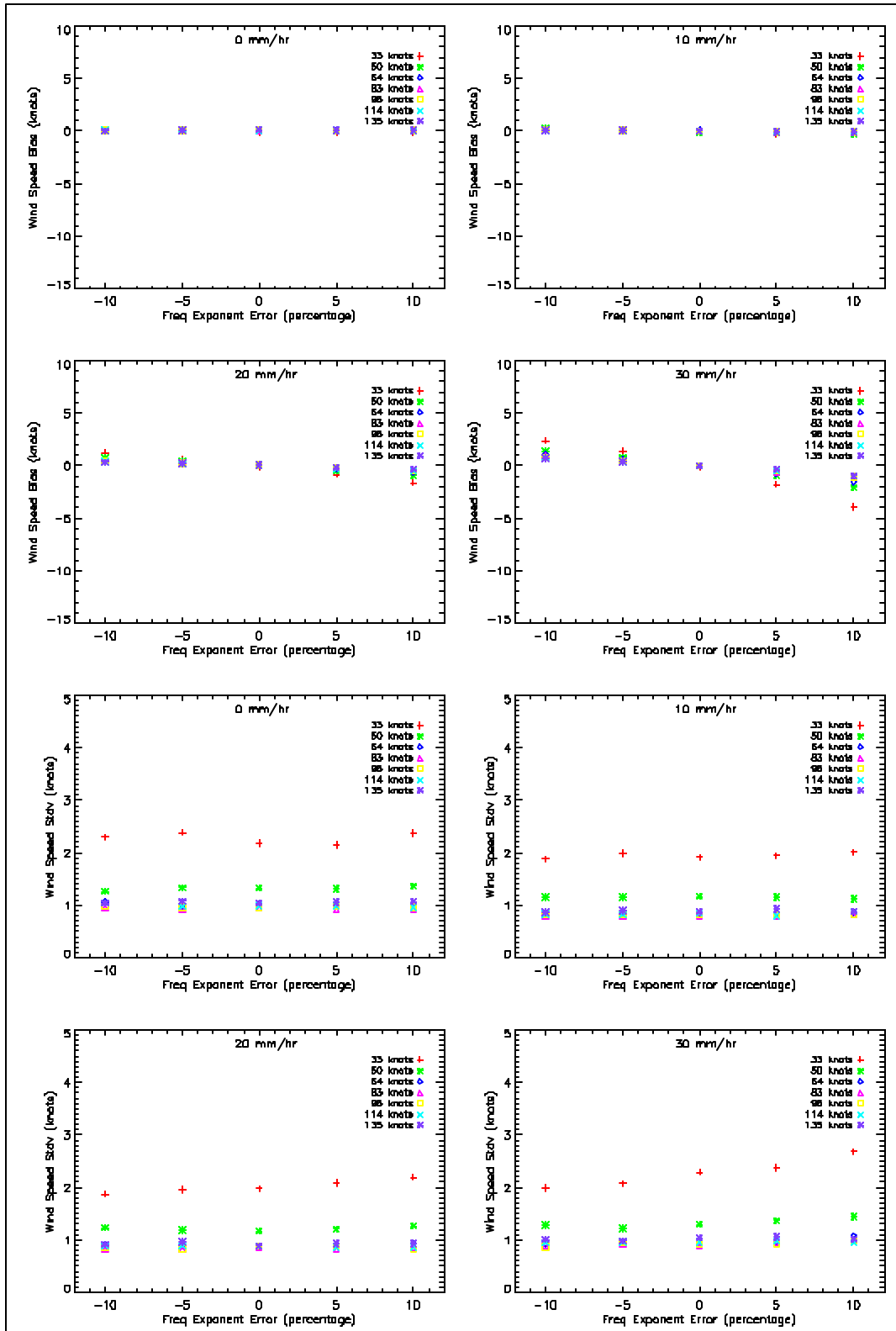**Figure 27: Errors in the rain retrievals caused by errors in frequency exponential coefficient in the rain model.**

Figure 28: Errors in the wind retrievals caused by errors in frequency exponential coefficient in the rain model.

3.4   Bathymetry Analysis

A key concern raised by HRD and NHC is the accuracy of the SFMR wind speed retrievals in shallow water. The concern is that in shallow water shoaling and other effects may cause over estimation of the ocean surface winds. Unfortunately, very little data has been collected that can concretely answer this question. As a start, the JHT SFMR team performed an initial analysis of Hurricane Rita flight on 23 September, 2005. Figure 30 displays the bathymetry for the region of Gulf of Mexico visited during the Rita flight. Figure 30 plots the flight track color coded based on the SFMR ocean surface wind speed retrievals. The bathymetry is still shown by the gray scale. Several legs were flown over regions with depths less than 50 m. Unfortunately, very little in situ measurement of the ocean surface wind field were available that could be used to discern between real changes in the ocean surface wind speed and bathymetry effects on the SFMR retrievals. Nevertheless, the SFMR retrievals were collocated with the bathymetry data.

Figure 31 plots collocated SFMR wind speed retrievals and bathymetry data. For this case, the wind retrievals appear to fluctuate with the bathymetry. A correlation analysis was performed on all the data binned in 10 m depth bins to determine if there was some consistent relationship between the bathymetry and the SFMR wind speed retrievals. The opposite result (although not statistically significant) was found. That is, the wind speed tended to decrease with decreasing water depth (negative correlation). The results are given in Table 3.

Of course, without knowledge of the actual surface wind speed, these results cannot be interpreted with any confidence.   The purpose of showing these plots and results, however, is to demonstrate that if targeted flight legs were flown, it may be possible to determine at what depths does the bathymetry affect the SFMR retrievals and to what extent. Figure 32 presents a proposed flight track. The legs are long enough to allow the GPS dropsonde splash point to be determined such that the aircraft can fly over the each splash point. The goal would be to execute a lawn mower pattern sampling water depths from 50 m down to 10 m and collecting in situ wind measurements with the GPS dropsondes. Over flying the drops is important to ensure accurate comparisons since the bathymetry effects may be small. This pattern should be executed in gale, storm and hurricane force wind conditions and rain-free conditions if possible.
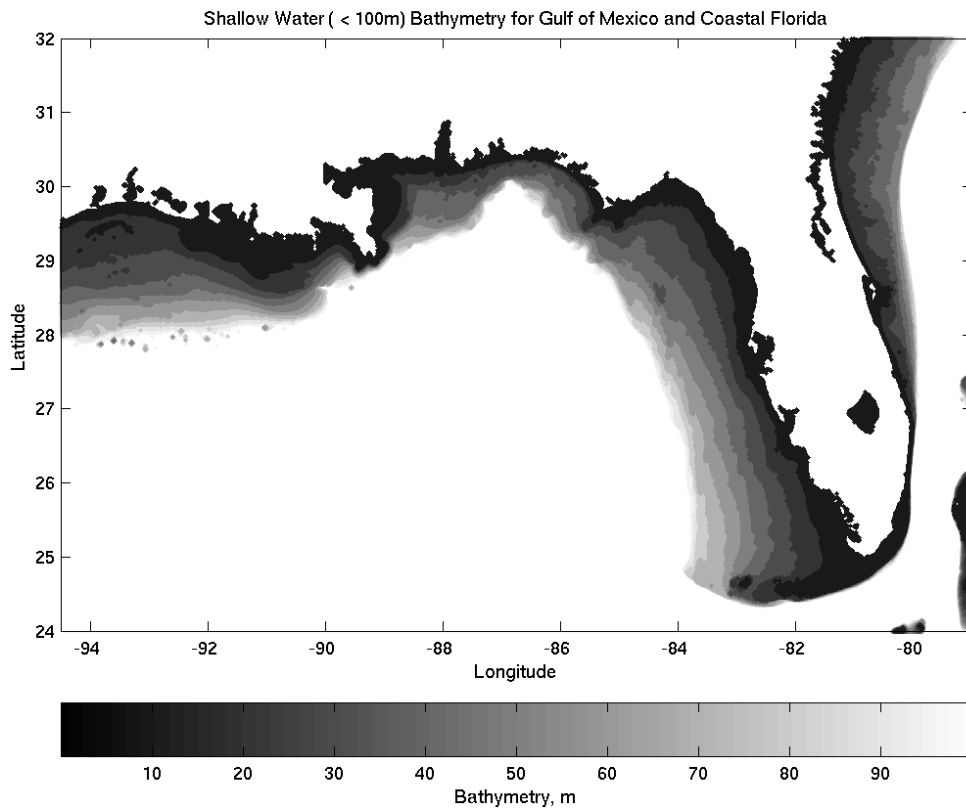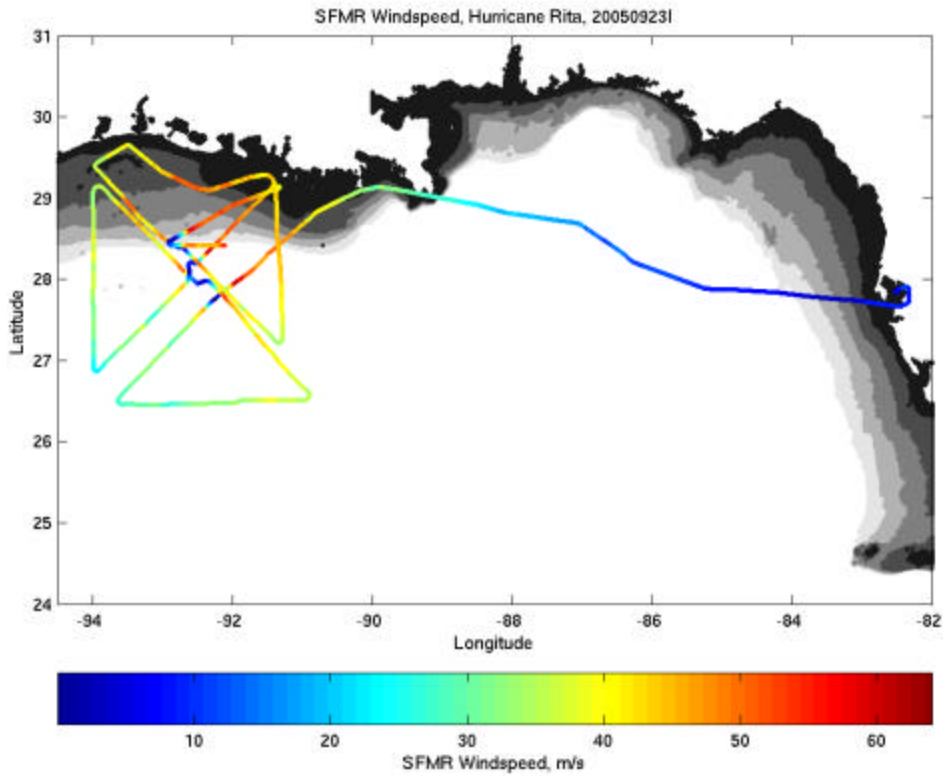
Figure 29: Bathymetry image of Gulf of Mexico.

Figure 30: Flight track through Hurricane Rita on 23 September 2005. The flight track is color coded according to the SFMR ocean wind speed estimates and bathymetry is shaded (10 m intervals).
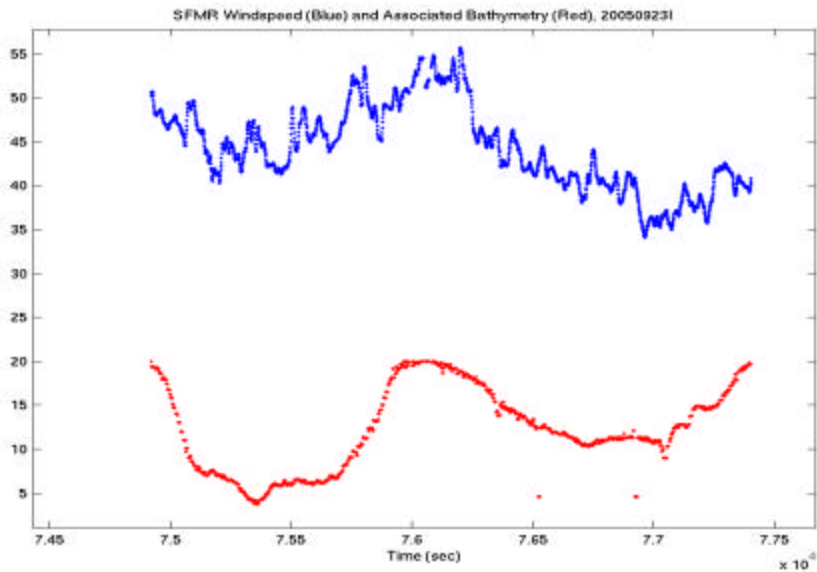

Figure 31: Collocated SFMR wind speed retrievals and bathymetry data are plotted during a flight through Hurricane Rita.

Table 3: Correlation analysis between the SFMR wind speed retrievals and water depth (wind speeds were greater than 25 m/s).

Depth	Number of Retrievals	Correlation Coefficient
D < 10m	1764	-0.55
10m < D < 20m	3187	-0.23
20m < D < 30m	1886	-0.05
30m < D < 40m	1358	0.03
40m < D < 50m	749	0.16
50m < D < 60m	1134	-0.43
60m < D < 70m	599	-0.04
70m < D < 80m	422	-0.27
80m < D < 90m	341	0.05
90m < D < 100m	208	-0.07
100m < D	9156	0.31

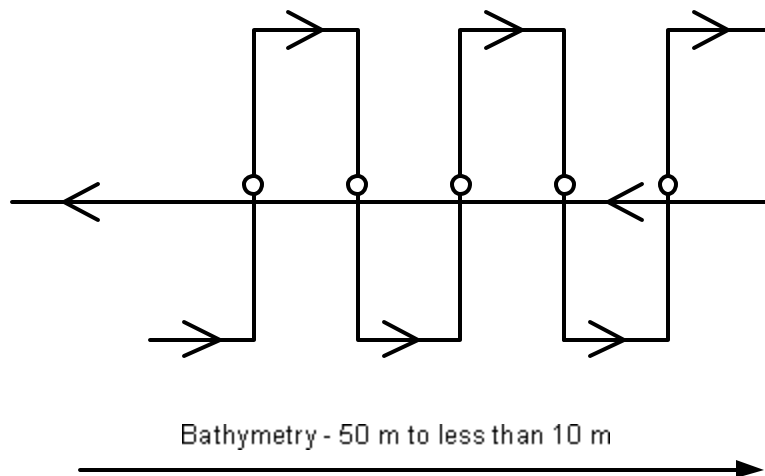Bathymetry - 50 m to less than 10 m

Figure 32: Proposed flight track to analyze bathymetry effects. Circles represent GPS dropsonde splash points.

4   Second Year – Building Upwards

Over the next year, the SFMR system is scheduled for integration on the 53rd Air Force Reserve WC-130 aircraft. Once deployed on this aircraft, an observational system will be in place to provide measurements of the ocean surface wind speed with coverage and resolution never before achieved. Our first year effort has identified areas that over the next year that need some improvement to maximize this potential. As was discussed in section 3, the retrieval process relies on tight agreement between the measurements and the GMF. Due to the nature of the problem, the wind and rain retrievals are coupled. Therefore it is critical to address and solve the known problems with the rain model and further validate the wind model. Remote Sensing Solutions, along with its NOAA partners, is positioned well to meet this need.

Beginning in August 2006, Remote Sensing Solutions will begin processing the 2005 and 2006 IWRAP measurements as part of a separate NOAA effort. IWRAP not only provides continuous and accurate mapping of the precipitation field as discussed in section 3, but also provides complete profiles of the atmospheric boundary layer winds in the presence of precipitation and the ocean surface wind field. Collocated on the same aircraft as the AOC SFMR, these IWRAP measurements will provide an unprecedented data set to improve and verify the SFMR GMF (rain and wind models).

With the 2006 data, the JHT SFMR team will tackle the bathymetry problem and provide guidance as to the use of the SFMR retrievals in shallow waters and near shore. The team will continue to work with NOAA AOC and ProSensing to further improve, validate and automate the calibration / tuning procedures. New methods for estimating the SST currently under study will be evaluated and tested for use with the SFMR retrieval process. Through these efforts we believe that the current 6 to 8 knot maximum uncertainty in the SFMR wind retrievals can be reduced to approximately 3 knots.

The JHT SFMR team will also work to improve the retrieval process. The current SFMR retrieval process does not permit negative rain rates. Statistically in rain free regions, negative rain solutions should occur due to measurement noise. By modifying the algorithm to permit negative rain, the current bias in the rain retrievals at very low rain rates will be removed and the algorithm will also converge upon its solution quicker.

Following this effort, advanced wind products shall be developed to provide the forecasters with real-time estimates of wind radii, maximum sustained winds, surface to flight level wind ratios, and more. RSS will incorporate these products into a real-time data system to make these products available to forecasters and other users who need them, and in the location and format that they are most useful.